Lipid Transfer Proteins and PI4KIIα Initiate Nuclear p53-Phosphoinositide Signaling

Noah D. Carrillo[1,2,4], Mo Chen[1,3,4], Tianmu Wen[1], Poorwa Awasthi[1], Colin Sterling[1,2], Dhruv Brahmbhatt[1,2], Vincent L. Cryns[1,2,5,*] and Richard A. Anderson[1,5,*]

[1]University of Wisconsin Carbone Cancer Center, University of Wisconsin-Madison, School of Medicine and Public Health; 1111 Highland Avenue, Madison, WI 53705, USA
[2]Department of Medicine, University of Wisconsin-Madison, School of Medicine and Public Health; 1111 Highland Avenue, Madison, WI 53705, USA
[3]Current Address: Department of Pharmacology, Joint Laboratory of Guangdong-Hong Kong Universities for Vascular Homeostasis and Diseases, SUSTech Homeostatic Medicine Institute, School of Medicine, Southern University of Science and Technology, Shenzhen 518055, China
[4]Co-first authors
[5]These authors contributed equally to this work
[*]Correspondence: vlcryns@medicine.wisc.edu; raanders@wisc.edu

Summary 250 max

Phosphoinositide (PIP_n) messengers are present in non-membranous regions of nuclei where they are assembled into a phosphatidylinositol (PI) 3-kinase (PI3K)/Akt pathway that is distinct from the cytosolic membrane-localized pathway. In the nuclear pathway, PI kinases/phosphatases bind the p53 tumor suppressor protein (wild-type and mutant) to generate p53-PIP_n complexes (p53-PIP_n signalosome) that activate Akt by a PI3,4,5P_3-dependent mechanism in non-membranous regions of the nucleus. This pathway is dependent on a source of nuclear PIP_ns that is poorly characterized. Here we report that a subset of PI transfer proteins (PITPs), which transport PI between membranes to enable membrane-localized PIP_n synthesis, also interact with p53 in the nucleus upon genotoxic stress. Class I PITPs (PITPα/β) specifically supply the PI required for the generation of p53-PIP_n complexes and subsequent signaling in the nucleus. Additionally, the PI 4-kinase PI4KIIα binds to p53 and the PITPs to catalyze the formation of p53-PI4P. p53-PI4P is then sequentially phosphorylated to synthesize p53-PIP_n complexes that regulate p53 stability, nuclear Akt activation and genotoxic stress resistance. In this way, PITPα/β and PI4KIIα bind p53 and collaborate to initiate p53-PIP_n signaling by mechanisms that require PI transfer by PITPα/β and the catalytic activity of PI4KIIα. Moreover, the identification of these critical upstream regulators of p53-PIP_n signaling point to PITPα/β and PI4KIIα as potential therapeutic targets in this pathway for diseases like cancer.

Key words

Phosphoinositide; PITP; PI4KIIα; p53; PI4,5P_2; PI3,4,5P_3; nucleus; cell stress; Akt

In Breif

Phosphatidylinositol transfer proteins and a PI 4-kinase initiate nuclear p53-PIP_n signaling in membrane-free regions.

Introduction

Phosphoinositide (PIP_n) lipids are synthesized from phosphatidylinositol (PI) in membranes by PIP-metabolizing enzymes, including kinases and phosphatases, to produce a second messenger network comprised of seven distinct isomers that play key roles in many cellular pathways[1]. Cytosolic class I PI 3-kinases (PI3Ks) catalyze the synthesis of PI3,4,5P_3, which leads to the recruitment and activation of the serine/threonine kinases phosphoinositide-dependent kinase 1 (PDK1), mTOR Complex 2 (mTORC2), and Akt at membranes[2-8]. Akt in turn phosphorylates many substrates, such as forkhead box O (FOXO) proteins, tuberous sclerosis complex 2 (TSC2), and BCL2-associated agonist of cell death (BAD), to promote cell growth and inhibit apoptosis[4]. This membrane-localized PI3K/Akt pathway is often hyperactivated in cancer and class I PI3K inhibitors are currently in the clinic[9, 10].

Akt is also activated in the nucleus[11-16]. Recent studies have identified a non-membranous nuclear PI3K/Akt pathway dependent on p53[17, 18], a tumor suppressor frequently mutated in cancer, resulting in gain-of-function oncogenic acitivities[19, 20]. In this nuclear pathway, wild-type and mutant p53 are sequentially modified by PIP_ns and their associated PIP kinases/phosphatases. The type I PI4P 5-kinase α (PIPKIα) directly interacts with p53 and generates the p53-PI4,5P_2 complex (p53-PIP_n signalosome) in response to stress[18]. PI5P4Kβ has also been functionally linked to p53 as deletion of both genes is lethal in mice, but the mechanism is poorly defined[21]. The nuclear PI 3-kinase IPMK (inositol polyphosphate multikinase) acts on p53-PI4,5P_2 to synthesize p53-PI3,4,5P_3 complexes, which then recruit and activate Akt in the non-membranous

nucleoplasm[17, 18]. The nuclear Akt pathway is insensitive to PI3K inhibitors in the clinic[17], highlighting its therapeutic importance.

Although multiple PIP_ns and PIP kinases/phosphatases are present in the nucleoplasm[16, 22-24], their function and regulation are poorly characterized compared to PIP_n signaling at cytosolic membranes. Specifically, prior studies have demonstrated the synthesis of PI in the ER, which is transported from the ER to other membranes, and shuttled between membranes by a family of lipid transfer proteins, the phosphatidylinositol transfer proteins (PITPs)[25]. To date, research has focused on the cytosolic function of PITPs[26-28]. Intriguingly, PITPβ was suggested to interact with p53[29], prompting us to investigate the functional role of PITPs in regulating the synthesis of p53-PIP_n complexes. Here we demonstrate that the highly homologous class I PITPs interact with p53 in the nucleus upon genotoxic stress and are specifically required to generate p53-PIP_n complexes. Additionally, a PI 4-kinase, PI4KIIα, binds to both p53 and the PITPs and is also required to initiate p53-PIP_n complex formation and nuclear p53-PIP_n signaling. PITPα/β and PI4KIIα collaborate to synthesize p53-PI4P complexes that are sequentially phosphorylated by PIP kinases or dephosphorylated by phosphatases to regulate p53 stability, nuclear Akt activation and stress resistance. These findings also implicate PITPα/β and PI4KIIα as therapeutic targets to regulate the nuclear p53-PIP_n pathway.

Results

p53 interacts with class I PITPs in the nucleus

The reported interaction of PITPβ and p53 in a proteomic screen[29] suggests that PITPs may play a functional role in generating nuclear p53-PIP_n complexes. To explore this, we investigated the interaction of p53 with all five PITPs using multiple approaches.

The PITP family is composed of five members that are subdivided into two classes that exchange PI for PC (Class I, the single domain PITPα and PITPβ isoforms) or PI for phosphatidic acid (PA) (Class II, the single domain PITP cytoplasmic 1 (PITPNC1) and the multi-domain PITP membrane-associated 1 and 2 (PITPNM1 and PITPNM2) isoforms with C-terminal extensions)[25] (Fig. 1a). The PITP-p53 interactions were first examined by immunoprecipitation (IP). Class I, but not class II PITPs, bound mutant p53 ($p53^{mt}$), and these interactions were increased by genotoxic stress (Fig. 1b-d,f,g). Of note, the PITPα antibody had partial cross-reactivity with PITPβ but not beyond the class I PITPs (Extended Data Fig. 1a). These IP interactions were recapitulated by *in vitro* binding studies with recombinant PITPα/β and p53 proteins demonstrating a high-affinity, saturable binding of class I PITPs to p53 (Extended Data Fig. 1b-e) Moreover, the small heat shock proteins (sHSPs) Hsp27 and αB-crystallin, which stabilize the p53-PIP_n complex[18], were also detected as stress-regulated components of the PITPα/β-p53 complex (Fig. 1b,e,f,h,i).

Proximity ligation assay (PLA) is an established approach to detect protein-protein interactions and posttranslational modifications (PTMs) *in situ*[30, 31]. Class I PITPs (PITPα and PITPβ), but not class II PITPs (PITPNCI, PITPNM1 and PITPNM2), associated with $p53^{mt}$ and wild-type p53 ($p53^{wt}$) in the nucleus as indicated by PLA foci, and their association was enhanced by cisplatin (Fig. 1j,k and Extended Data Fig. 2a-c).

Interestingly, PITPα/β-p53 PLA complexes were present in the nucleoplasm in regions distinct from the nuclear envelope (Fig. 1l, Extended Data Fig. 2d-f, and Supplementary Video 1-2). Despite their previously reported confinement to the cytosol[25, 26], PITPα/β were observed in the nucleus under basal conditions and chemotharputic stress resulted in their nuclear accumulation, supporting the PLA data (Extended Data Fig. 3a). Notably, the association of PITPα/β with $p53^{wt}$ was minimal under basal conditions and dramatically increased by stress, while PITPα/β associated constitutively with $p53^{mt}$ with a modest increase in response to stress. Regardless of p53 mutational status, stress-responsive PITPα/β-p53 complexes were detected in all cell lines examined (Fig. 1m and Extended Data Fig. 3b-n). Moreover, p53 directly bound class I PITPs, but not PITPNC1, with low nM K_d as determined by microscale thermophoresis (MST) (Fig. 1n), underscoring the specificity of these interactions.

PITPα/β are required for p53-PIP_n complex generation

As PITPα/β bind to p53 in the nucleus, we examined the potential role of PITPα/β in regulating the PIP_n associations with p53, which stabilize p53[18]. The p53-PIP_n complexes[17, 18] were first analyzed by PLA. Single or combined knock down (KD) of PITPα/β, but not PITPNC1, reduced or largely eliminated, respectively, $p53^{mt}$-PI4,5P_2 and $p53^{mt}$-PI3,4,5P_3 complexes detected by PLA; combined KD of PITPα/β disrupted $p53^{mt}$-PIP_n complexes to a similar degree as p53 KD (Fig. 2a-c and Extended Data Fig. 4a,b). Similar results were observed in $p53^{wt}$ cells: individual or combined PITPα/β KD inhibited $p53^{wt}$-PI4,5P_2 and $p53^{wt}$-PI3,4,5P_3 complexes (Fig. 2d-f).

We next identified and quantified the cisplatin-induced PIP_n isoforms linked to p53 by p53-IP followed by simultaneous Western blotting (WB) with antibodies (Abs) against specific PIP_n isomers detected with fluorescently labeled secondary Abs (IP fluorescent-WB) (Fig. 2g and Extended Data Fig. 4c). KD of PITPα or PITPβ markedly reduced the PI4P, $PI4,5P_2$ and $PI3,4,5P_3$ that co-IPed with $p53^{mt}$ in response to genotoxic stress, while the combined KD virtually eliminated all PIP_ns associated with $p53^{mt}$ (Fig. 2h-k). Similar observations were made in cells with $p53^{wt}$: single or combined PITPα/β KD also inhibited cisplatin-stimulated $p53^{wt}$-$PI4,5P_2$ complex formation (Fig. 2l,m). Consistent with the reported role of PIP_ns in stabilizing p53[18], KD of PITPα or PITPβ, but not PITPNC1, modestly reduced $p53^{mt}$ levels in cells treated with cisplatin, while the combined KD of PITPα and PITPβ robustly suppressed $p53^{mt}$ levels under basal and stress conditions (Extended Data Fig. 4d). Reduced p53 levels after combined PITPα/β KD were not rescued by the MDM2 inhibitor Nutlin 3a[32], suggesting a MDM2-independent mechanism (Extended Data Fig. 4e). Moreover, the robust induction of $p53^{wt}$ by cisplatin was inhibited by individual PITPα/β KD and abrogated by combined PITPα/β KD (Extended Data Fig. 4f). The PIP_n antibody approach was confirmed using radiolabeled [^{3}H]-inositol which is specifically incorporated into PIP_ns and inositol phosphates[33]. [^{3}H]-inositol was added to the culture media and p53 was IPed from these cells, resolved via WB, and excised from the gel, resulting in a high degree of consistency between antibody reactivity and [^{3}H] counts (Fig. 3a-b and Extended Data Fig. 4g). These findings indicate that class I PITPα and PITPβ play a key role in the stress-responsive coupling of PIP_ns to $p53^{wt}$ and $p53^{mt}$ proteins. The p53 associated PIP_n, identifiable by monoclonal antibody and [^{3}H]-inositol

lableing marks a unique and stable protein-lipid complex that persists through denaturation and SDS-PAGE analysis.

PI4KIIα interacts with p53 and cooperates with PITPα/β to synthesize p53-PI4P

As PITPα/β were reported to cooperate with PI 4-kinases (PI4Ks) to synthesize PI4P[25, 34, 35], we postulated that PI4Ks act in concert with PITPα/β to generate p53-PI4P. To explore this, each of the four human PI4Ks[36] were individually KDed and PLA was used to quantify changes in the p53-PI4P complexes. KD of PI4KIIα specifically suppressed basal and cisplatin-stimulated p53-PI4P levels, while combined KD of PI4KIIα and PI4KIIIα reduced p53-PI4P levels to the same degree as PI4KIIα KD alone (Fig. 4a,b and Extended Data Fig. 5a). p53-PI4P is the substrate for PIPKIα to synthesize p53-PI4,5P_2, which stabilizes p53[18]. Consistent with its role in generating p53-PI4P, PI4KIIα KD, but not KD of other PI4Ks, inhibited cisplatin-stimulated p53 levels (Fig. 4c). Moreover, KD of PI4KIIα mirrored the effects of PIPKIα KD in suppressing p53 induction by cisplatin, and combined KD of PI4KIIα and PIPKIα was equivalent to either individual KD with regard to p53 levels (Fig. 4d). In contrast to PI4KIIα KD which reduced p53-PI4P levels, KD of PIPKIα enhanced p53-PI4P levels (Fig. 4e,f and Extended Data Fig. 5b). p53-PI4P synthesis requires the catalytic activity of PI4KIIα as the PI4KIIα inhibitors (PI-273 and NC03)[37, 38] prevented p53-PI4P generation and subsequent formation of p53-PI4,5P_2 (Fig. 4g and Extended Data Fig. 5c-e). To further define these p53-PIP_n complexes, we utilized a p53 C-terminal domain (CTD) polybasic domain mutant ($p53^{6Q}$), which disrupts PI4,5P_2 binding to p53 (wild-type and oncogenic mutants)[17, 18]. In this context, the $p53^{6Q}$ mutant formed more abundant $p53^{6Q}$-PI4P complexes than the corresponding wild-type CTD

domain p53 proteins (Extended Data Fig. 6a,b). However, the $p53^{6Q}$-PI4P complexes were not phosphorylated further to $p53^{6Q}$-PI3,4,5P_3 complexes (Extended Data Fig. 6c,d), likely due to disrupted binding of PIPKIα and/or IPMK, which interact with the p53 C-terminus[17, 18]. Conventional PIP_n binding to p53 relies on a weak electrostatic interaction between a polybasic and positively charged surface of p53 and the acidic and negatively charged headgroup of the PIP_n. This manner of interaction often encompasses the PIP_n headgroup and is ablated by harsh denaturing conditions. The $p53^{6Q}$ mutant loses key basic amino acids and disrupts conventional PIP_n binding[18]. However, the stable PI4P association with p53 is enhanced by the $p53^{6Q}$ mutation as determined by PLA, persists through denaturation as demonstrated by WB, and retains headgroup accessibility and signaling competency as previously shown[17].

In addition, PI4KIIα co-IPed with $p53^{mt}$ and $p53^{wt}$, and these interactions were enhanced by genotoxic stress (Fig. 4h). PI4KIIIα also co-IPed with $p53^{mt}$ and $p53^{wt}$, (Fig. 4h) but PI4KIIIα KD did not affect p53 or p53-PI4P levels or enhance the effects of PI4KIIα KD (Fig. 4a-c). Recombinant PI4KIIα bound to p53, PITPα, and PITPβ with saturatable kinetics and low nM affinity (Extended Data Fig. 7a-d), consistent with a specific and direct interaction. Interestingly, the PI4KIIα-PITPβ interaction was enhanced by the addition of p53, suggesting a ternary PI4KIIα:PITPβ:p53 protein complex that contributes to p53 stability (Fig. 4i and Extended Data Fig. 7e-g). These findings indicate that PI4KIIα binds to p53 with high affinity and, together with PITPα/β, specifically synthesizes p53-PI4P and contributes to p53 stabilization by generating the precursor for p53-PI4,5P_2 (Fig. 4j).

PITPα/β regulate p53-PIP$_n$ signalosome formation and nuclear Akt activation to inhibit stress-induced apoptosis

The p53-PIP$_n$ signalosome is regulated by cellular stress, leading to the formation of p53-PI3,4,5P$_3$ complexes that recruit and activate Akt in the nucleus and protect cells from stress-induced apoptosis[17]. The identification of class I PITPs as upstream regulators of p53-PIP$_n$ complex assembly implicates these lipid transfer proteins in nuclear Akt activation. Consistent with this concept, individual KD of PITPα or PITPβ, but not PITPNC1, suppressed stress-induced nuclear Akt activation quantified by nuclear pAkt^{S473} IF, an established approach[17], while combined PITPα/β KD resulted in a more robust reduction of pAkt^{S473} (Fig. 5a,b). These results were confirmed in MDA-MB-231 cells by WB (Extended Data Fig. 8a). Similar results were obtained with multiple human cancer cell lines expressing different p53^{mt} proteins (Fig. 5c-e). KD of p53^{mt}, PITPα or PITPβ, but not PITPNC1, moderately reduced cell viability under basal conditions and sensitized MDA-MB-231 cells to cisplatin treatment, while combined KD of PITPα/β further decreased cell viability (Fig. 5f,g). Consistent with these results, knockout (KO) of PITPβ or KD of PITPα had modest effects on cisplatin-induced cell death, while combined PITPβ KO and PITPα KD enhanced the cytotoxicity of cisplatin (Fig. 5h and Extended Data Fig. 8b). Individual or combined PITPα/β KD had similar effects on cisplatin sensitivity in four additional breast cancer cell lines expressing different p53^{mt} or p53^{wt} proteins (Extended Data Fig. 8c-j). The cytotoxicity of p53^{mt} KD and individual or combined PITPα/β KD was associated with a corresponding increase in caspase 3 activity (Fig. 5i and Extended Data Fig. 8k-m), indicating that PITPα/β KD triggers apoptosis and sensitizes cells to genotoxic stress. These findings underscore the critical

role of PITPα/β in regulating nuclear Akt activation, which confers resistance to genotoxic stress-induced apoptosis.

PITPα/β-mediated p53-PIP_n signaling requires PI transfer activity

As PITPα/β exchange PI for PC, we investigated whether the PI transfer activity of these PITPs was required to regulate p53 levels and nuclear Akt activation. For this, we utilized the PITPα/$β^{T59D}$ mutant that specifically disrupts PI binding[39-41]. Ectopically expressed HA-tagged PITPα/$β^{wt}$ interacted with $p53^{wt}$ and mutant $p53^{R175H}$, while the corresponding PITPα/$β^{T59D}$ mutants exhibited impaired interaction with p53 (Fig. 6a and Extended Data Fig. 9a-c). Moreover, the reduction in the stress-induced p53 protein and nuclear $pAkt^{S473}$ levels by combined PITPα and PITPβ KD using distinct siRNAs targeting their 3'-UTR was rescued by expression of $PITPα^{wt}$, but not mutant $PITPα^{T59D}$ (Fig. 6b-d). Notably, nuclear $pAkt^{S473}$ levels correlated with the content of re-expressed $PITPα^{wt}$, but not mutant $PITPα^{T59D}$ (Fig. 6e,f), indicating that these phenotypes are dose-dependent.

The cytotoxicity and sensitization to cisplatin-induced apoptosis by combined PITPα/β KD using the 3'-UTR targeting siRNAs were partly rescued by re-expressing $PITPα^{wt}$ but not the PITPα/$β^{T59D}$ mutant (Fig. 6g-i). These results demonstrate that the PI transfer activity of class I PITPs regulates their interaction with p53, p53 stability, and subsequent nuclear Akt activation. Combined PITPα/β KD also inhibited EGF-stimulated cell invasion, and these effects were partly restored by re-expressing $PITPα^{wt}$ but not the $PITPα^{T59D}$ mutant (Extended Data Fig. 9d,e), consistent with reports that PITPs contribute to EGF signaling[42]. The data indicate that PITPα/β regulate cell growth, invasion, and protection

against genotoxic stress (Fig. 6j), although elucidation of the underlying mechanisms will require additional investigation.

Discussion

Here, we reveal an unexpected role for class I PITPα/β in generating nuclear p53-PIP_n complexes that initiate nuclear PIP_n signaling. Although the existence of nuclear PIP_ns and their role in the cell cycle[43], oxidative stress[16, 44-49] , and the DNA damage response[17, 50-52] is supported by growing evidence[16], the molecular regulators of nuclear PIP_ns in regions devoid of membranes have been enigmatic[53]. PITPs have a well-established role in transporting PI from the endoplasmic reticulum to membranes, enabling membrane-localized PIP_n signaling via PIP kinases, phosphatases, and phospholipases[25, 54-58]. The findings presented here demonstrate that class I PITPs directly bind p53 with high affinity in the nucleus in response to genotoxic stress. As such, these data expand the roles of the PITPα/β lipid transport activities that were thought to act solely at cytosolic membranes and establish their mechanistic roles in generating nuclear p53-PIP_n complexes.

PITPα/β, but not other PITP family members, bind directly to $p53^{wt}$ and $p53^{mt,}$ and these interactions are stimulated by cell stress. This complex also includes the small heat shock proteins (Hsp27 and αB-crystallin), which stabilize p53[18]. PITPα/β binding to p53 is necessary for the linkage of PIP_ns with p53 (p53-PIP_n signalosome). Once the p53-PIP_n complex is formed, it is stable, detected by PIP_n isomer antibodies, and acted on by multiple PIP kinases and phosphatases, indicating that the myo-inositol head group is accessible, a characteristic that distinguishes these complexes from conventional protein-

PIP_n binding[17, 18, 31]. The p53-PIP_n signalosome culminates in the formation of p53-PI3,4,5P_3 complexes that, in turn, recruit and activate Akt in the nucleus, conferring resistance to stress-induced apoptosis[17]. However, PITPs also contribute to the canonical membrane-localized PI3K/Akt pathway[59], so the observed differences in cellular phenotypes by PITPα/β KD likely reflect some contribution of both the canonical and the nuclear PI3K/Akt pathways. These PITPα/β activities require PI binding, underscoring the critical functional role of lipid transport as a mechanism to establish nuclear PIP_ns.

The ability of wild-type PITPα, but not the PI binding-defective mutant, to rescue the phenotype of combined PITPα/β KD suggests a functional redundancy between the class I PITPs. This is consistent with previous reports that either PITPα or PITPβ is sufficient to rescue the phenotype of double PITPα/β knockout in a PI-binding dependent manner[39, 60]. PITPα/β also binds to PI4KIIα, and the addition of p53 protein increases the affinity between PITPs and PI4KIIα, which supports formation of a ternary complex. As both PITPα/β and PI4KIIα are required to generate p53-PI4P, these data point to a functional collaboration between PITPα/β and PI4KIIα in initiating nuclear p53-PIP_n signaling that is reminiscent of their roles in generating PI4P in the membrane-localized pathway[34, 35].

Remarkably, PITPα/β and PI4KIIα regulate the association of PIP_ns to p53 in a manner that is inconsistent with traditional protein-PIP_n interactions. Conventional protein-PIP_n interactions are electrostatic in nature and are disrupted by denaturation and SDS-PAGE, yet p53-PIP_n complexes remain intact following these interventions[17, 18]. Previous studies have demonstrated that the $p53^{6Q}$ CTD mutant has diminished binding to PIP_ns[17, 18], but the $p53^{6Q}$-PI4P complex is enhanced, further distinguishing these complexes from

conventional p53-PIP_n binding. Perhaps most significantly, the p53-linked PIP_ns maintain signaling competency as they are modified by kinases and phosphatases and remain detectable via antibody recognition of their *myo*-inositol headgroup or [^{3}H]-inositol radiolabeling. In contrast to p53-PIP_n complexes, most protein-PIP_n interactions involve direct binding of the headgroup to protein domains precluding the lipid from kinase or phosphatase modification[61, 62], underscoring this unique characteristic of p53-PIP_n complexes. The data presented here indicate that PIP_n second messengers, beginning with PI4P, are linked to p53 by the combined activities of PITPα/β and PI4KIIα. The resulting p53-PI4P is acted on by PIP kinases and phosphatases such that the p53-PI3,4,5P_3 functions as a nuclear messenger to recruit PDK1, mTORC2, and Akt. Notably, each of these proteins is known to interact with the PIP_n head group. In the case of mutant p53 proteins, p53 activation may contribute to its oncogenic gain-of-function activity by activating nuclear Akt and suppressing apoptosis, whereas this prosurvival activity may counteract the proapoptotic function of wild-type p53 and represent a novel mechanism for wild-type p53 to confer stress-resistance consistent with prior reports of its ability to regulate metabolism, oxidative stress and DNA damage[63]. These findings suggest a “third messenger” pathway[17] with p53 as the founding member whereby PIP_n second messengers are linked to cellular proteins in membrane-free regions and modified by PIP kinases/phosphatases to regulate their function (Fig. 6j). Given the critical role of class I PITPs in initiating nuclear phosphoinositide signaling, which attenuates cellular stress and apoptosis, these findings also point to these PITPs and PI4KIIα as potential therapeutic targets in a variety of diseases including cancer.

ACKNOWLEDGMENTS

We thank Dr. Adrea Galmozzi for discussions and comments and Lance Rodenkirch for technical support. N.D.C. is supported by a National Institutes of Health T32 Training Grant 5T32ES007015-43 to the Molecular and Environmental Toxicology graduate training program at UW-Madison. M.C. is supported by grants 32400577, 2023A1515110237, JCYJ20240813094605008, and D2301007. This work was supported in part by a National Institutes of Health grant R35GM134955 (R.A.A.), R01CA286492 (R.A.A. & V.L.C.), Department of Defense Breast Cancer Research Program grants W81XWH-21-1-0129 (V.L.C.), HT9425-23-1-0553 (V.L.C.), and HT9425-23-1-0554 (R.A.A.), and a grant from the Breast Cancer Research Foundation (V.L.C.).

AUTHOR CONTRIBUTIONS

M.C., N.D.C, T.W., V.L.C., and R.A.A. designed the experiments. N.D.C., M.C., T.W., P.A., T.J.W., C.S., and D.B. performed the experiments. N.D.C., M.C., T.W., V.L.C., and R.A.A. wrote the manuscript.

DECLARATION OF INTERESTS

Authors declare that they have no competing interests.

Experimental Procedures

Cell culture and constructs

A549, BT-549, Cal33, HCT116, HS578T, MDA-MB-231, SUM159, SUM1315, HEK293FT, and MCF-10A cells were purchased from ATCC. MCF10A cells were cultured in DMEM/F12 (#11330-032, Invitrogen) supplemented with 10% fetal bovine serum (#SH30910.03, Hyclone), 1% penicillin/streptomycin (#15140-122, Gibco), 20 ng/mL EGF (#CC-4107, Lonza), 0.5 mg/mL Hydrocortisone (#H4001, Sigma), 100 ng/mL Cholera toxin (#C-8052, Sigma), and 10 µg/mL Insulin (#I-1882, Sigma). The other cells were maintained in DMEM (#10-013-CV, Corning) supplemented with 10% fetal bovine serum (#SH30910.03, Hyclone) and 1% penicillin/streptomycin (#15140-122, Gibco). The Flag-tagged p53 constructs and corresponding PIP_n-binding-defective 6Q mutants in this work have been described previously[18]. The HA-tagged wild-type PITPα/β constructs and PI-binding deficient mutants T59D[39] were purchased from Genscript. Plasmids were transfected into mammalian cells using Lipofectamine™3000, (#L3000015, Thermo Fisher Scientific) according to the manufacturer's instructions. Typically, 2-5 µg of DNA and 6-10 µl of lipid were used for transfecting cells in 6-well plates. Cells with at least 80% transfection efficiency were used for further analysis.

Antibodies and reagents

Monoclonal antibodies against p53 (clone DO-1, #SC-126, Santa Cruz Biotechnology), p53 (clone 7F5, #2527, Cell Signaling), $pAkt^{S473}$ (clone 193H12, #4058, Cell Signaling), HA-tag (clone C29F4, #3724, Cell Signaling), Flag-tag (clone D6W5B, #14793, Cell

Signaling), GAPDH (clone 0411, #sc-47724, Santa Cruz Biotechnology), Lamin B2 (clone D8P3U, #12255, Cell Signaling), EGFR (clone D6B6, #2085, Cell Signaling), HSP27 (clone D6W5V, #95357, Cell Signaling), and polyclonal antibodies against PITPα (#16613-1-AP, ThermoFisher), PITPβ (#ab127563, abcam), PITPNC1 (IF, #ab222078, abcam), PITPNC1 (WB, #NBP2-19842, Novus), PITPNM1 (#26983-1-AP, Proteintech), PITPNM2 (#PA5-48616, Invitrogen), pAkt^{T308} (#9275, Cell Signaling), PI4KIIα (#NBP2-44158, Novus), PI4KIIIα (#4902S, CST), PI4KIIβ (#PA5-82133, Thermo), PI4KIIIβ (#ab134756, abcam), and αB-Crystallin (#ADI-SPA-223-F, Enzo) were used in this study. For conventional immunostaining and PLA analysis of phosphoinositides, anti-PI4P (#Z-P004), PI4,5P_2 (#Z-P045), and PI3,4,5P_3 (#Z-P345) antibodies were purchased from Echelon Biosciences. For immunoblotting analyses, antibodies were diluted at a 1:1000 ratio except for p53 (clone DO-1, 1:5000) and GAPDH (clone 0411, 1:5000). For immunoprecipitation, antibody-conjugated agarose was purchased from Santa Cruz Biotechnology, including agarose-conjugated antibodies against p53 (#sc-126AC), PITPα/β (#sc-398050AC), HA-tag (#sc-7392AC), and Flag-tag (#sc-166355AC). For immunostaining analyses and proximity ligation assay (PLA), antibodies were diluted at a 1:100 ratio. The nuclear envelope marker (Alexa Fluor®488 Lamin A/C, clone 4C11, #8617, Cell Signaling, 1:200) examined subnuclear regions. For the knockdown (KD) experiments, the ON-TARGETplus siRNA SMARTpool with four siRNAs in combination against human p53 (#L-003329-00), PITPα (#L-018010-00), PITPβ (#L-006459-01), and PITPNC1 (#L-012476-02) were purchased from Dharmacon. Non-targeting siRNA (#D-001810-01, Dharmacon) was used as a control. For the KD and rescue experiments, pooled-siRNAs targeting the 3'UTR of PITPα (sense 5'-

AGGCAACUUUCGAUUCCUUACUGUA-3' and antisense 5'-UACAGUAAGGAAUCGAAAGUUGCCU-3'; sense 5'-CCGUCUCUCUCCAUUGUGUUCCGAU-3' and antisense 5'-AUCGGAACACAAUGGAGAGAGACGG-3') and pooled-siRNAs targeting the 3'UTR of PITPβ (sense 5'- GAGUGAACAACAAUCUGACCAGUAU-3' and antisense 5'-AUACUGGUCAGAUUGUUGUUCACUC-3'; sense 5'- CUACAAAGCUGAUGAAGAC-3' and antisense 5'-GUCUUCAUCAGCUUUGUAG-3') were purchased from Thermo Fisher Scientific. The siRNAs were delivered to cells by RNAiMAX reagent (#13778150, Thermo Fisher Scientific), and KD efficiency was determined by immunoblotting. KD efficiency greater than 80% was required to observe phenotypic changes in the study. Cisplatin (#NC1706394, Fisher Scientific), etoposide (#S1225, Sellekchem), Erastin (#S7242, Selleckchem), tert-Butylhydroquinone (tBHQ, #SPCM-T1540-06, Spectrum), and hydroxyurea (HU, #1332000, Millipore Sigma) were used as cellular stressors. Nutlin 3a (#S8059, Sellekchem), PI-273 (#AOB37765, aobious), and NC03 (#AOB17420, aobious) were also used.

Immunoprecipitation and immunoblotting

Cells were removed from the medium after the indicated treatment, washed three times with ice-cold PBS, and lysed in an ice-cold RIPA lysis buffer system (#sc-24948, Santa Cruz Biotechnology) with 1 mM Na_3VO_4, 5 mM NaF, and 1x protease inhibitor cocktail (#11836153001, Roche). The cell lysates were then sonicated followed by incubation at 4°C with continuous rotation for 1 h and centrifuged at maximum speed for 10 min to collect the supernatant. The protein concentration in the supernatant was measured by

the Bradford protein assay (#5000201, BIO-RAD). All antibodies were diluted at a 1:1000 ratio for immunoblotting unless otherwise indicated. For immunoprecipitation, 0.5-1 mg of protein was incubated with 20 μl of antibody-conjugated agarose (Santa Cruz Biotechnology) at 4°C for 24 h. After washing three times with PBST (PBS with 0.1% Tween 20), the protein complex was eluted with SDS sample buffer and boiled at 95°C for 10 min. For immunoblotting, 5-20 μg of protein were loaded. For immunoblotting of immunoprecipitated complexes, horseradish peroxidase (HRP)-conjugated antibodies were used to avoid non-specific detection of immunoglobulin in the immunoprecipitated samples. HRP-conjugated p53 (#sc-126HRP), PITPα (#sc-13569HRP), and PITPβ (#sc-390500HRP) antibodies were purchased from Santa Cruz Biotechnology. Immunoblots were developed by Odyssey Imaging System (LI-COR Biosciences), and the intensity of protein bands was quantified using ImageJ. Statistical data analysis was performed with Microsoft Excel, using data from at least three independent experiments.

Fluorescent IP-WB

Cells were lysed in a RIPA lysis buffer system[17] and lysates were incubated with 20 μl anti-p53 (#sc-126 AC, Santa Cruz Biotechnology) mouse monoclonal IgG antibody-conjugated agarose at 4°C for 24 h. Normal immunoglobulin (IgG)-conjugated agarose was used as a negative control (#sc-2343, Santa Cruz Biotechnology). The protein complex was eluted with SDS sample buffer and boiled at 95°C for 10 min. For immunoblotting, 5-20 μg of protein were loaded. The protein complexes were analyzed via WB as described above. For double fluorescent IP-WB detecting p53-PI4P/PI4,5P_2/PI3,4,5P_3 complexes, anti-p53 rabbit monoclonal IgG antibody (clone 7F5,

#2527, Cell Signaling) at 1:2000 dilution and anti-PI4P mouse monoclonal IgM antibody (#Z-P004, Echelon Biosciences), PI4,5P_2 mouse monoclonal IgM antibody (#Z-P045, Echelon Biosciences), or PI3,4,5P_3 mouse monoclonal IgM antibody (#Z-P345, Echelon Biosciences) at 1:1000 dilution were mixed in blocking buffer with 0.02 % Sodium Azide and incubated with the membrane at 4°C overnight. For the secondary antibody incubation, goat anti-rabbit IgG antibody conjugated with IRDye 800CW fluorophore (#926-32211, LI-COR) and goat anti-mouse IgM antibody conjugated with IRDye 680RD fluorophore (#926-68180, LI-COR) at 1:10000 dilution were mixed in blocking buffer with 0.01 % SDS and 0.1% Tween 20 and incubated with the membrane at room temperature for 2 h. The images were subsequently acquired simultaneously using the 700 and 800 nm wavelength channels on the Odyssey Fc Imaging System (LI-COR Biosciences). Statistical data analysis was performed with Microsoft Excel, using data from at least three independent experiments.

Immunofluorescence (IF) and Confocal Microscopy

For immunofluorescence studies, cells were grown on coverslips coated with 0.2 % gelatin (#G9391, Millipore Sigma). Cells were fixed with 4% paraformaldehyde (PFA) (#sc-281692, Santa Cruz Biotechnology) for 20 min at room temperature, then washed three times with PBS. Next, the cells were permeabilized with 0.3% Triton-X100 for 30 min to permeate the nuclear envelope thoroughly and were rewashed three times with PBS. The cells were then blocked with 1% BSA in PBS for one hour at room temperature. After blocking, cells were incubated with primary antibodies overnight at 4ºC. The cells were then washed three times with PBS and incubated with fluorescent-conjugated

secondary antibodies (Molecular Probes) for 1 hour at room temperature. After secondary antibody incubation, the cells were washed three times. Then the coverslips were removed from the dishes, air-dried for 10 min at room temperature and mounted in Prolong™ Glass Antifade Mountant with NucBlue™ Stain (#P36985, Thermo Fisher Scientific). The images were taken by a Leica SP8 3xSTED Super-Resolution Microscope, a point scanning confocal, and a 3xSTED super-resolution microscope using LASX software (Leica Microsystems). All images were acquired using the 100X objective lens (N.A. 1.4 oil). The z-stack images were taken with each frame of 0.2 μm thickness. For quantification, the mean fluorescent intensity of channels in each cell was measured by LASX. GraphPad Prism Version 9.4.1 generated quantitative graphs. The images were processed using ImageJ. The correlation of double staining channels was quantified by GraphPad Prism using Pearson's correlation coefficient (Pearson's r), ranging between 1 and −1.

Proximity Ligation Assay (PLA)

PLA was utilized to detect *in situ* protein-protein/PIP_n interaction or close proximity, as previously described[17, 18, 31]. After fixation and permeabilization, cells were blocked before incubation with primary antibodies as in routine IF staining. The cells were then processed for PLA (#DUO92101, MilliporeSigma) according to the manufacturer's instruction and previous publications[17, 18, 31]. Post-PLA slides were further processed for immunofluorescent staining against the nuclear membrane marker (Lamin A/C, #8617, Cell Signaling). After washing, the slides were processed and imaged as indicated in the IF section above. The Leica SP8 confocal microscope detected PLA signals as discrete

punctate foci and provided the intracellular localization of the complex. ImageJ was used to quantify the nuclear PLA foci.

Crystal Violet Cell Viability Assay

In 96-well plates, 5×10^4 cells/well of MDA-MB-231, MDA-MB-231^{Cas9}, BT549, SUM159, or SUM1315 cells were transfected with control siRNAs or siRNAs targeting p53, PITPα, PITPβ, PITPNC1, or the combination of PITPα and PITPβ as indicated for 48 h. For the KD rescue experiments, MDA-MB-231 cells were transfected with control siRNAs or siRNAs targeting 3'UTR of PITPα and PITPβ for 24 h. Next, the cells were transfected with HA-tagged wild-type PITPα or its PI-binding deficient T59D mutant PITPα for another 24 h. The cells were then treated with the control vehicle or 30 μM cisplatin for 24 h, and the cells were subsequently fixed with 4% PFA and stained with 0.2% Crystal Violet. After washing, the plates were air-dried at room temperature and imaged using the EVOS M5000 Imaging System (ThermoFisher Scientific). The dye was extracted from the cells with 10% acetic acid and quantified by measuring the absorbance at 570 nm using a Synergy HTX Multi-Mode Microplate reader.

Caspase 3 Activity Assay

In 6-well plates, 1×10^6 cells/well of MDA-MB-231, BT549, SUM159, or SUM1315 were transfected with control siRNAs or siRNAs targeting p53, PITPα, PITPβ, PITPNC1, or the combination of PITPα and PITPβ as indicated for 48 h. For the KD rescue experiments, MDA-MB-231 cells were transfected with control siRNAs or siRNAs targeting 3'UTR of PITPα and PITPβ for 24 h. Then, the cells were transfected with either HA-tagged wild-

type PITPα or its PI-binding deficient T59D mutant PITPα for another 24 h, followed by treatment with a control vehicle or 30 μM cisplatin for 24 h. Next, the cells were lysed and processed for a Caspase 3 activity assay following the manufacturer's instructions (#E-13183, Thermo Fisher Scientific). The fluorescence was read at excitation/emission 342/441 nm using a Synergy HTX Multi-Mode Microplate reader.

Microscale Thermophoresis (MST) Assay

The microscale thermophoresis (MST) assay was used to calculate the binding affinities of purified recombinant proteins (p53 (#81091, Active Motif), PITPα (#ab101666, Abcam), PITPβ (#LS-C794864, LSBio), PITPNC1 (#LS-G33119-10, LSBio) PI4KIIα (lab-made)) and other contributing factors *in vitro* as previously described[64]. Following the manufacturer's instruction, the target protein was fluorescently labeled using a Monolith Protein Labeling kit (RED-NHS 2nd Generation MO-L011, Nano Temper). Then, sequential titration of unlabeled ligand proteins or PI (#840042P, Avanti), was made in a Tris-based MST buffer and mixed with an equal volume of fluorescently labelled target protein prepared at 10 nM concentration in the same MST buffer, making the final target protein at a constant concentration of 5 nM and the ligand-protein or lipid as the gradient. For PI cofactor analysis, target proteins were mixed with 1 μM PI before ligand proteins. The target–ligand mixtures were loaded into Monolith NT.115 series capillaries (MO-K022, Nano Temper), and the MST traces were measured using Monolith NT.115 pico. The binding affinity was auto-generated using MO Control v.1.6 software.

***In vitro* binding assay**

The recombinant proteins p53 (#81091, Active Motif), PITPα (#ab101666, Abcam), PITPβ (#ab101091, Abcam), and PI4KIIα (lab made) were used for *In Vitro* binding assays. The binding assay was performed in PBS by incubating a constant amount of p53 or PI4KIIα with an increasing amount of p53, PITPα/β, or PI4KIIα in the presence of 20 µl anti-p53 antibody-conjugated agarose (#sc-126AC, Santa Cruz). After incubating overnight at 4°C, unbound proteins were removed by washing three times with PBST, and the protein complex was analyzed by immunoblotting.

Nuclear Fractionation

Nuclear fractionation was used to analyze compartmentalized protein expression. MDA-MB-231 cells were processed using the NE-PER nuclear and cytoplasmic extraction reagents (#78833, Thermo) according to the manufacturer's instructions. Cells were manually removed from their culture dishes into suspension, and the cytosolic extraction reagent was used to isolate cytosolic fractions. Then, the nuclear extraction reagent was used to produce the nuclear fraction.

Lenti-CRISPR Gene Editing

CRISPR-Cas9 genome editing was used to knock out the gene encoding PITPβ in MDA-MB-231 cells. First, a Cas9 expressing stable cell line was generated by transducing cells with viral particles (#LVCAS9BST, Sigma Aldrich) at the multiplicity of infection (MOI) of 0.5. Transduction was performed in complete media containing 8µg/mL polybrene. After 24 h incubation, Cas9-expressing cells were selected with 10µg/mL blasticidin (#DSB12150; Dot Scientific) for 1 week, and expression was confirmed. To generate

PITPβ KO cells, viral particles containing the guide RNA sequence for PITPβ (5'-CAATCATCCTCACGAATGC-3') and negative control (5'-CGCGATAGCGCGAATATATT-3') were purchased from Sigma Aldrich. Sequences were cloned into LV21 lentiviral vectors (Sigma Aldrich). Cas9-expressing cells were then transduced with viral particles at a MOI of 0.5 and incubated for 24 h. Transduction was performed in the presence of 8μg/mL polybrene in complete media. Media was removed 24 h after viral transduction and 1500 μg/mL geneticin (#10131035; Sigma Aldrich) was added for selection. After 1 week of selection in antibiotics, single cells were isolated in the 96-well tissue culture dish by BD FACS AriaII.

Transwell Invasion Assay

The bottom polycarbonate filter surface of a 6.5 mm diameter insert with 8 μm pores in a 24-well plate (#3422, Corning) was coated with 10 μg/ml of Laminin (#CC095, Millipore Sigma) diluted in PBS for 3 h at 37°C. MDA-MB-231 cells were transiently transfected with control siRNAs or siRNAs targeting the 3'UTR of both PITPα and PITPβ for 24 h. Then, the cells were transfected with either HA-tagged wild-type PITPα or its PI-binding deficient T59D mutant PITPα. After 24 h, cells were serum starved for an additional 24 h. Next, $5x10^4$ transfected cells were suspended in 200 μl serum-free medium containing 0.5% BSA and then were plated in the upper insert chamber in 500 μl serum-free medium with 0.5% BSA. 10 ng/ml EGF was added to the lower chamber. Cells were allowed to invade for 16 h at 37°C. Cells on the bottom of the filter were then fixed with 4% PFA and stained with 0.2% Crystal Violet. The stained cells were imaged using the EVOS M5000 Imaging System (ThermoFisher Scientific). At the end of the assay, the dye was extracted

by 10% acetic acid from the cells and quantified by measuring the optical density at 570 nm using a Synergy HTX Multi-Mode Microplate reader.

[^{3}H]*myo*-inositol Metabolic Labeling

Cells were split and cultured in low serum Opti-MEM (#31985070, Thermo) supplemented with 10% dialyzed FBS with a 10,000 mw cut-off (#F0392, Sigma) and 1% Pen/strep (#15140-122, Gibco) to minimize inositol in the culture media. In 10 cm dishes, 0.5×10^6 MDA-MB-231 cells were seeded to achieve ~5% confluency the following day. 24 h after plating, cells were treated with either 1.322 μM (25 μCi/mL) of [^{3}H]*myo*-inositol (#NET1156005MC, PerkinElmer) or unlabeled *myo*-inositol (#J60828.22, Thermo) and allowed to uptake the metabolic label for 48 h. For KD experiments, PITPα/β siRNAs were added and recovered as normal and fresh [^{3}H]*myo*-inositol supplemented media was used to replace the transfection media. 24 h after siRNA transfection (72 h after original plating), cells were treated with control vehicle or 30 μM cisplatin for another 24 h. Labeled and unlabeled cells were then lysed and p53 was immunoprecipitated as described in *immunoprecipitation and* immunoblotting, before performing SDS-PAGE or $CHCl_3$/MeOH extraction as indicated. For extraction, MeOH:$CHCl_3$ (2:1) was added to RIPA cell lysates to form the protein precipitate. Soluble phases in MeOH and $CHCl_3$ were aspirated out and the protein flake was dried using a speed vacuum. Protein samples were then resuspended and solubilized in PBS with sonication. SDS-PAGE samples were excised from the gel and each lane was either further sectioned or treated as a whole and dissolved in 30% H_2O_2 before liquid scintillation counting (LSC). Dissolved gel samples or resuspended protein samples from the $CHCl_3$/MeOH extraction were added to LSC vials with LSC cocktail (#6013319, PerkinElmer) before being processed by

PerkinElmer Tri-Carb 4910 TR liquid scintillation analyzer. Analysis and DPM calculation were automated using QuantaSmart software.

Statistics and Reproducibility

Two-tailed unpaired *t*-tests were used for pair-wise significance, and one-way ANOVA was used for group significance with Bonferroni's multiple comparisons test used for significance within grouped samples. We note that no power calculations were used. Sample sizes were determined based on previously published experiments where significant differences were observed[17, 18]. We used at least three independent experiments or biologically independent samples for statistical analysis.

Resource and Data Availability

To allow others to replicate and build on this work, we will make all materials, data, and associated protocols available to readers in a public repository upon publication.

References

1. Hammond, G.R.V. & Burke, J.E. Novel roles of phosphoinositides in signaling, lipid transport, and disease. *Curr Opin Cell Biol* **63**, 57–67 (2020).
2. Fruman, D.A. *et al.* The PI3K Pathway in Human Disease. *Cell* **170**, 605–635 (2017).
3. Hoxhaj, G. & Manning, B.D. The PI3K-AKT network at the interface of oncogenic signalling and cancer metabolism. *Nat Rev Cancer* **20**, 74–88 (2020).
4. Manning, B.D. & Toker, A. AKT/PKB Signaling: Navigating the Network. *Cell* **169**, 381–405 (2017).
5. Burke, J.E., Triscott, J., Emerling, B.M. & Hammond, G.R.V. Beyond PI3Ks: targeting phosphoinositide kinases in disease. *Nat Rev Drug Discov*, 1–30 (2022).
6. Currie, R.A. *et al.* Role of phosphatidylinositol 3,4,5-trisphosphate in regulating the activity and localization of 3-phosphoinositide-dependent protein kinase-1. *Biochem J* **337 (Pt 3)**, 575–583 (1999).
7. Liu, P. *et al.* PtdIns(3,4,5)P3-Dependent Activation of the mTORC2 Kinase Complex. *Cancer Discov* **5**, 1194–1209 (2015).
8. Calleja, V. *et al.* Intramolecular and intermolecular interactions of protein kinase B define its activation in vivo. *PLoS Biol* **5**, e95 (2007).
9. Altomare, D.A. & Testa, J.R. Perturbations of the AKT signaling pathway in human cancer. *Oncogene* **24**, 7455–7464 (2005).
10. Kondapaka, S.B., Singh, S.S., Dasmahapatra, G.P., Sausville, E.A. & Roy, K.K. Perifosine, a novel alkylphospholipid, inhibits protein kinase B activation. *Mol Cancer Ther* **2**, 1093–1103 (2003).
11. Kikani, C.K. *et al.* Proliferative and antiapoptotic signaling stimulated by nuclear-localized PDK1 results in oncogenesis. *Science signaling* **5**, ra80 (2012).
12. Shiraishi, I. *et al.* Nuclear targeting of Akt enhances kinase activity and survival of cardiomyocytes. *Circ Res* **94**, 884–891 (2004).
13. Fu, W. & Hall, M.N. Regulation of mTORC2 Signaling. *Genes (Basel)* **11** (2020).
14. Martelli, A.M. *et al.* The emerging multiple roles of nuclear Akt. *Biochim Biophys Acta* **1823**, 2168–2178 (2012).
15. Liu, L. *et al.* DNA-PK promotes activation of the survival kinase AKT in response to DNA damage through an mTORC2-ECT2 pathway. *Science signaling* **15**, eabh2290 (2022).
16. Chen, M. *et al.* The nuclear phosphoinositide response to stress. *Cell Cycle* **19**, 268–289 (2020).
17. Chen, M. *et al.* A p53-phosphoinositide signalosome regulates nuclear AKT activation. *Nat Cell Biol* **24**, 1099–1113 (2022).
18. Choi, S., Chen, M., Cryns, V.L. & Anderson, R.A. A nuclear phosphoinositide kinase complex regulates p53. *Nat Cell Biol* **21**, 462–475 (2019).
19. Muller, P.A. & Vousden, K.H. p53 mutations in cancer. *Nat Cell Biol* **15**, 2–8 (2013).
20. Hassin, O. & Oren, M. Drugging p53 in cancer: one protein, many targets. *Nat Rev Drug Discov* **22**, 127–144 (2023).
21. Emerling, B.M. *et al.* Depletion of a putatively druggable class of phosphatidylinositol kinases inhibits growth of p53-null tumors. *Cell* **155**, 844–857 (2013).

22. Cocco, L. *et al.* Synthesis of polyphosphoinositides in nuclei of Friend cells. Evidence for polyphosphoinositide metabolism inside the nucleus which changes with cell differentiation. *Biochem J* **248**, 765–770 (1987).
23. Boronenkov, I.V., Loijens, J.C., Umeda, M. & Anderson, R.A. Phosphoinositide signaling pathways in nuclei are associated with nuclear speckles containing pre-mRNA processing factors. *Mol Biol Cell* **9**, 3547–3560 (1998).
24. Blind, R.D. *et al.* The signaling phospholipid PIP3 creates a new interaction surface on the nuclear receptor SF-1. *Proc Natl Acad Sci U S A* **111**, 15054–15059 (2014).
25. Ashlin, T.G., Blunsom, N.J. & Cockcroft, S. Courier service for phosphatidylinositol: PITPs deliver on demand. *Biochim Biophys Acta Mol Cell Biol Lipids* **1866**, 158985 (2021).
26. Shadan, S. *et al.* Dynamics of lipid transfer by phosphatidylinositol transfer proteins in cells. *Traffic* **9**, 1743–1756 (2008).
27. Morgan, C.P. *et al.* Differential expression of a C-terminal splice variant of phosphatidylinositol transfer protein beta lacking the constitutive-phosphorylated Ser262 that localizes to the Golgi compartment. *Biochem J* **398**, 411–421 (2006).
28. van Tiel, C.M. *et al.* The Golgi localization of phosphatidylinositol transfer protein beta requires the protein kinase C-dependent phosphorylation of serine 262 and is essential for maintaining plasma membrane sphingomyelin levels. *J Biol Chem* **277**, 22447–22452 (2002).
29. Huang, Y. *et al.* Global tumor protein p53/p63 interactome: making a case for cisplatin chemoresistance. *Cell Cycle* **11**, 2367–2379 (2012).
30. Oliveira, F.M.S. *et al.* Detection of post-translational modifications using solid-phase proximity ligation assay. *N Biotechnol* **45**, 51–59 (2018).
31. Chen, M., Horn, H.T., Wen, T., Cryns, V.L. & Anderson, R.A. Assessing In Situ Phosphoinositide-Protein Interactions Through Fluorescence Proximity Ligation Assay in Cultured Cells. *Methods Mol Biol* **2251**, 133–142 (2021).
32. Vassilev, L.T. *et al.* In vivo activation of the p53 pathway by small-molecule antagonists of MDM2. *Science* **303**, 844–848 (2004).
33. Wilson, M.S.C. & Saiardi, A. Importance of Radioactive Labelling to Elucidate Inositol Polyphosphate Signalling. *Top Curr Chem (Cham)* **375**, 14 (2017).
34. Lete, M.G., Tripathi, A., Chandran, V., Bankaitis, V.A. & McDermott, M.I. Lipid transfer proteins and instructive regulation of lipid kinase activities: Implications for inositol lipid signaling and disease. *Adv Biol Regul* **78**, 100740 (2020).
35. Grabon, A., Bankaitis, V.A. & McDermott, M.I. The interface between phosphatidylinositol transfer protein function and phosphoinositide signaling in higher eukaryotes. *J Lipid Res* **60**, 242–268 (2019).
36. Boura, E. & Nencka, R. Phosphatidylinositol 4-kinases: Function, structure, and inhibition. *Experimental cell research* **337**, 136–145 (2015).
37. Li, J. *et al.* PI-273, a Substrate-Competitive, Specific Small-Molecule Inhibitor of PI4KIIalpha, Inhibits the Growth of Breast Cancer Cells. *Cancer Res* **77**, 6253–6266 (2017).
38. Sengupta, N. *et al.* A large scale high-throughput screen identifies chemical inhibitors of phosphatidylinositol 4-kinase type II alpha. *J Lipid Res* **60**, 683–693 (2019).

39. Xie, Z., Hur, S.K., Zhao, L., Abrams, C.S. & Bankaitis, V.A. A Golgi Lipid Signaling Pathway Controls Apical Golgi Distribution and Cell Polarity during Neurogenesis. *Dev Cell* **44**, 725–740 e724 (2018).
40. Tilley, S.J. *et al.* Structure-function analysis of human [corrected] phosphatidylinositol transfer protein alpha bound to phosphatidylinositol. *Structure* **12**, 317–326 (2004).
41. Alb, J.G., Jr., Gedvilaite, A., Cartee, R.T., Skinner, H.B. & Bankaitis, V.A. Mutant rat phosphatidylinositol/phosphatidylcholine transfer proteins specifically defective in phosphatidylinositol transfer: implications for the regulation of phospholipid transfer activity. *Proc Natl Acad Sci U S A* **92**, 8826–8830 (1995).
42. Kauffmann-Zeh, A. *et al.* Requirement for phosphatidylinositol transfer protein in epidermal growth factor signaling. *Science* **268**, 1188–1190 (1995).
43. Stallings, J.D., Tall, E.G., Pentyala, S. & Rebecchi, M.J. Nuclear translocation of phospholipase C-delta1 is linked to the cell cycle and nuclear phosphatidylinositol 4,5-bisphosphate. *J Biol Chem* **280**, 22060–22069 (2005).
44. Jones, D.R. *et al.* Nuclear PtdIns5P as a transducer of stress signaling: an in vivo role for PIP4Kbeta. *Mol Cell* **23**, 685–695 (2006).
45. Bua, D.J., Martin, G.M., Binda, O. & Gozani, O. Nuclear phosphatidylinositol-5-phosphate regulates ING2 stability at discrete chromatin targets in response to DNA damage. *Sci Rep* **3**, 2137 (2013).
46. Yokogawa, T. *et al.* Evidence that 3 '-phosphorylated polyphosphoinositides are generated at the nuclear surface: use of immunostaining technique with monoclonal antibodies specific for PI 3,4-P-2. *Febs Lett* **473**, 222–226 (2000).
47. Li, W. *et al.* Star-PAP control of BIK expression and apoptosis is regulated by nuclear PIPKIalpha and PKCdelta signaling. *Mol Cell* **45**, 25–37 (2012).
48. Mellman, D.L. *et al.* A PtdIns4,5P2-regulated nuclear poly(A) polymerase controls expression of select mRNAs. *Nature* **451**, 1013–1017 (2008).
49. Tanaka, K. *et al.* Evidence that a phosphatidylinositol 3,4,5-trisphosphate-binding protein can function in nucleus. *Journal of Biological Chemistry* **274**, 3919–3922 (1999).
50. Wang, Y.H. *et al.* DNA damage causes rapid accumulation of phosphoinositides for ATR signaling. *Nat Commun* **8**, 2118 (2017).
51. Wang, Y.H. & Sheetz, M.P. When PIP(2) Meets p53: Nuclear Phosphoinositide Signaling in the DNA Damage Response. *Front Cell Dev Biol* **10**, 903994 (2022).
52. Wang, Y.H. & Sheetz, M.P. Transcription-independent functions of p53 in DNA repair pathway selection. *Bioessays* **45**, e2200122 (2023).
53. Barlow, C.A., Laishram, R.S. & Anderson, R.A. Nuclear phosphoinositides: a signaling enigma wrapped in a compartmental conundrum. *Trends Cell Biol* **20**, 25–35 (2010).
54. Cockcroft, S. & Carvou, N. Biochemical and biological functions of class I phosphatidylinositol transfer proteins. *Biochim Biophys Acta* **1771**, 677–691 (2007).
55. Hunt, A.N., Clark, G.T., Attard, G.S. & Postle, A.D. Highly saturated endonuclear phosphatidylcholine is synthesized in situ and colocated with CDP-choline pathway enzymes. *J Biol Chem* **276**, 8492–8499 (2001).
56. Wang, Y., Sweitzer, T.D., Weinhold, P.A. & Kent, C. Nuclear localization of soluble CTP:phosphocholine cytidylyltransferase. *J Biol Chem* **268**, 5899–5904 (1993).
57. Tribble, E.K. *et al.* Quantitative profiling of the endonuclear glycerophospholipidome of murine embryonic fibroblasts. *J Lipid Res* **57**, 1492–1506 (2016).

58. Blunsom, N.J. & Cockcroft, S. Phosphatidylinositol synthesis at the endoplasmic reticulum. *Biochim Biophys Acta Mol Cell Biol Lipids* **1865**, 158471 (2020).
59. Cosker, K.E. *et al.* Regulation of PI3K signalling by the phosphatidylinositol transfer protein PITPalpha during axonal extension in hippocampal neurons. *J Cell Sci* **121**, 796–803 (2008).
60. Li, F.L. *et al.* Hippo pathway regulation by phosphatidylinositol transfer protein and phosphoinositides. *Nat Chem Biol* **18**, 1076–1086 (2022).
61. Lemmon, M.A. Phosphoinositide recognition domains. *Traffic* **4**, 201–213 (2003).
62. Lemmon, M.A. Membrane recognition by phospholipid-binding domains. *Nat Rev Mol Cell Biol* **9**, 99–111 (2008).
63. Kruiswijk, F., Labuschagne, C.F. & Vousden, K.H. p53 in survival, death and metabolic health: a lifeguard with a licence to kill. *Nat Rev Mol Cell Biol* **16**, 393–405 (2015).
64. Asmari, M., Ratih, R., Alhazmi, H.A. & El Deeb, S. Thermophoresis for characterizing biomolecular interaction. *Methods* **146**, 107–119 (2018).

FIGURE LEGEND

Figure 1. p53 interacts with the PITPs in the nucleus upon stress

a, Domains of PITP class I and II protein family members. PITD, PI transfer domain; FFAT, two phenylalanines in an acidic tract; DDHD, Asp-Asp-His-Asp motif; LNS2, Lipin/Nde1/Smp2 domain.

b-e, Co-IP of PITPα/PITPβ/Hsp27 with p53 from MDA-MB-231 cells treated with vehicle or 30 μM cisplatin for 24 h. PITPα IP-ed by p53 (**c**), PITPβ IP-ed by p53 (**d**), and Hsp27 IP-ed by p53 (**e**), as well as PITPNC1/PITPNM1/PITPNM2 were analyzed by WB. *p* value denotes two-sided paired t-test.

f-i, Co-IP of p53/Hsp27/αB-crystallin (αBC) with the shared epitope of PITPα/β from MDA-MB-231 cells treated with vehicle or 30 μM cisplatin for 24 h. p53 IP-ed by PITPα/β (**g**), Hsp27 IP-ed by PITPα/β (**h**), and αBC IP-ed by PITPα/β (**i**) were analyzed by WB. *p* value denotes two-sided paired t-test.

j-k, PLA of p53-PITPα/PITPβ/PITPNC1/PITPNM1/PITPNM2 in MDA-MB-231 cells treated with vehicle or 30 μM cisplatin for 24 h. The nuclear p53-PITP foci were quantified (**k**). n=3, 10 cells from each independent experiment. *p* value denotes two-sided paired t-test. See expanded images in Extended Data Fig. 2a.

l, PLA of p53-PITPα/PITPβ/PITPNC1/PITPNM1/PITPNM2 overlaid with the nuclear envelope marker Lamin A/C in MDA-MB-231 cells treated with vehicle or 30 μM cisplatin for 24 h. The nuclei were counterstained by DAPI. See expanded images in Extended Data Fig. 2e.

m, Co-IP of PITPα/PITPβ with p53 in BT549, Cal33, HS578T, SUM159, SUM1315 cells treated with vehicle or 30 μM cisplatin for 24 h. PITPα/PITPβ IPed by p53 (**n**) and

PITPNC1/PITPNM1/PITPNM2 were analyzed by WB. See expanded images in Extended Data Fig. 3j-n.

n, The interaction of recombinant fluorescently labelled p53 with other components was quantitated by MST assay. A constant concentration of fluorescently labelled p53 (5 nM) was incubated with increasing concentrations of non-labelled ligand with or without the addition of 1 μM PI and analyzed using a Monolith NT.115 pico, and the binding affinity was autogenerated by MO. Control v.1.6 software. Data are presented as the mean ± SD. For all panels, n=3 independent experiments.

Figure 2. PITPα/β regulate p53-PIP$_n$ complexes

a-c, MDA-MB-231 cells were transfected with control siRNAs or siRNAs against p53, PITPα, PITPβ, PITPNC1, or both PITPα and PITPβ. After 24 h, cells were treated with 30 μM cisplatin or vehicle for 24 h before being processed for PLA to detect p53-PI4,5P$_2$/-PI3,4,5P$_3$ complexes (**b,c**). n=3, 10 cells from each independent experiment. *p* value denotes ANOVA with Bonferroni's multiple comparisons test. See KD validation in Extended Data Fig. 4d and expanded images in Extended Data Fig. 4a,b.

d-f, A549 cells were transfected with control siRNAs or siRNAs against PITPα, PITPβ, or both PITPα and PITPβ. After 24 h, cells were treated with 30 μM cisplatin or vehicle for 24 h before being processed for PLA to detect p53-PI4,5P$_2$/PI3,4,5P$_3$ complexes (**e,f**). n=3, 10 cells from each independent experiment. *p* value denotes ANOVA with Bonferroni's multiple comparisons test. See KD validation in Extended Data Fig. 4f.

g, MDA-MB-231 cells were treated with 30 μM cisplatin or vehicle for 24 h before being processed for IP against p53. p53-bound PI4P/PI4,5P$_2$/PI3,4,5P$_3$ were examined by fluorescent WB. See quantification in Extended Data Fig. 4c.

h-k, MDA-MB-231 cells were transfected with control siRNAs or siRNAs against PITPα, PITPβ, or both PITPα and PITPβ. After 24 h, cells were treated with 30 μM cisplatin or vehicle for 24 h before being processed for IP against p53. p53-bound PI4P/PI4,5P_2/PI3,4,5P_3 were examined by fluorescent WB and quantified by ImageJ (**i-k**). *p* value denotes ANOVA with Bonferroni's multiple comparisons test. See KD validation in Extended Data Fig. 4d.

l-m, A549 cells were transfected with control siRNAs or siRNAs against PITPα, PITPβ, or both PITPα and PITPβ. After 24 h, cells were treated with 30 μM cisplatin or vehicle for 24 h before being processed for IP against p53. The PI4,5P_2 level on IPed p53 was quantified by ImageJ (**m**). *p* value denotes ANOVA with Bonferroni's multiple comparisons test. See KD validation in Extended Data Fig. 4f.

For all panels, n=3 independent experiments and data are represented as mean ± SD. Scale bar, 5 μm.

Figure 3. p53-PIP$_n$ complexes are validated by [^{3}H]-inositol lableing

a-b, MDA-MB-231 cells were cultured from low confluency in media containing [^{3}H]*myo*-inositol or unlabeled *myo*-inositol. After 72 h of growth to confluency, cells were treated with 30 μM cisplatin or vehicle for 24 h before being processed for IP against p53. p53 and PI4,5P_2 were confirmed by fluorescent WB (**a**) before samples were resolved by SDS-PAGE and the gel lane was excised and sectioned. Gel sections were then dissolved and analyzed by liquid scintillation counting (LSC) (**b**). n=3 independent experiments, error bar denotes SD, t-test, $p<0.01$*, $p<0.001$**. For all graphs, data are presented as the mean ± SD.

Figure 4. PI4KIIα interacts with p53 to generate p53-PI4P complexes

a-b, MDA-MB-231 cells were transfected with control siRNAs or siRNAs against PI4KIIIα, PI4KIIIβ, PI4KIIα, PI4KIIβ or both PI4KIIα and PI4KIIIα. After 24 h, cells were treated with 30 μM cisplatin or vehicle for 24 h before being processed for PLA to detect p53-PI4P complexes (**b**). n=3, 15 cells from each independent experiment. *p* value denotes ANOVA with Bonferroni's multiple comparisons test. See KD confirmation in Fig. 4c and expanded images in Extended Data Fig. 4a.

c, MDA-MB-231 cells were transfected with control siRNAs or siRNAs against PI4KIIIα, PI4KIIIβ, PI4KIIα, PI4KIIβ or both PI4KIIα and PI4KIIIα. After 24 h, cells were treated with 30 μM cisplatin or vehicle for 24 h before being processed for WB. p53 levels were quantified by ImageJ. *p* value denotes ANOVA with Bonferroni's multiple comparisons test.

d, A549 and MDA-MB-231 cells were transfected with control siRNAs or siRNAs against PI4KIIIα, PIPKIα or both PI4KIIα and PIPKIα. After 24 h, cells were treated with 30 μM cisplatin or vehicle for 24 h before being processed for WB. p53 levels were quantified by ImageJ. *p* value denotes ANOVA with Bonferroni's multiple comparisons test.

e,f, MDA-MB-231 and A549 cells were transfected with control siRNAs or siRNAs against PI4KIIIα, PIPKIα or both PI4KIIα and PIPKIα. After 24 h, cells were treated with 30 μM cisplatin or vehicle for 24 h before being processed for PLA to detect p53-PI4P complexes. n=3, 15 cells from each independent experiment. *p* value denotes ANOVA with Bonferroni's multiple comparisons test. See KD confirmation in Fig. 4d and expanded images in Extended Data Fig. 4b.

g, MDA-MB-231 cells were treated with vehicle or cisplatin in combination with DMSO as a control, PI-273, or NC03 for 24 h before being processed for PLA to detect p53-PI4,5P_2 complexes and analyzed using ImageJ. *p* value denotes two-sided paired t-test. n=3, 15 cells from each independent experiment. See expanded images in Extended Data Fig. 5e.

h, MDA-MB-231 and A549 cells were treated with 30 μM cisplatin or vehicle for 24 h before being processed for IP against p53. The PI4KIIIα, PI4KIIIβ, PI4KIIα, and PI4KIIβ levels IPed with p53 were analyzed by WB.

i, MDA-MB-231^{Cas9} cells with PITPβ KO and control non-targeted KO were transfected with control siRNAs or siRNAs against PI4KIIα, PITPα, or both PI4KIIα and PITPα. After 24 h, cells were treated with 30 μM cisplatin or vehicle for 24 h before being processed for WB.

j, Model showing PITPα/β cooperation with PI4KIIα in generating p53-PI4P complexes that participate in further signaling.

For all panels, n=3 independent experiments and data are represented as mean ± SD. Scale bar, 5 μm.

Figure 5. PITPα/β regulate p53-dependent nuclear Akt activation and cell survival

a-b, MDA-MB-231 cells were transfected with control siRNAs or siRNAs against PITPα, PITPβ, PITPNC1, or both PITPα and PITPβ. After 24h, cells were treated with 30 μM cisplatin or vehicle for 24 h before being processed for IF staining against pAkt^{S473}. The nuclear pAkt^{S473} levels were quantified by ImageJ (**b**). n=3, 15 cells from each independent experiment. *p* value denotes ANOVA with

Bonferroni's multiple comparisons test. Scale bar, 5 μm. See KD validation in Extended Data Fig. 4d.

c-e, BT-549, SUM159, and SUM1315 cells with the indicated p53 status were transfected with control siRNAs or siRNAs against both PITPα and PITPβ. After 24 h, cells were treated with 30 μM cisplatin or vehicle for 24 h before being processed for IF staining against $pAkt^{S473}$. The nuclei were counterstained by DAPI. The nuclear $pAkt^{S473}$ levels were quantified by ImageJ (**d**). n=3, 15 cells from each independent experiment. *p* value denotes two-sided paired t-test. Scale bar, 5 μm. The double KD of PITPα and PITPβ in SUM159 cells was validated by WB (**e**). See KD validation for BT-549 and SUM1315 cells in Extended Data Fig. 8h, j.

f-g, MDA-MB-231 cells were transfected with control siRNAs or siRNAs against p53, PITPα, PITPβ, PITPNC1, or both PITPα and PITPβ. After 24 h, cells were treated with 30 μM cisplatin or vehicle for 24 h before being processed for Crystal Violet viability assay. The cells were imaged by an EVOS M5000 microscope (**f**) and quantified based on the extracted dye using a plate reader (**g**). *p* value denotes ANOVA with Bonferroni's multiple comparisons test. Scale bar, 300 μm.

h, MDA-MB-231^{Cas9} cells with PITPβ KO and control non-targeted KO were transfected with control siRNAs or siRNAs against PITPα, PITPβ, or both PITPα and PITPβ. After 24 h, cells were treated with 30 μM cisplatin or vehicle for 24 h before being processed for Crystal Violet viability assay. The cells were imaged by an EVOS M5000 microscope. Scale bar, 300 μm. See quantification in Extended Data Fig. 8b.

i, MDA-MB-231 cells were transfected with control siRNAs or siRNAs against p53, PITPα, PITPβ, PITPNC1, or both PITPα and PITPβ. After 24h, cells were treated with 30 μM

cisplatin or vehicle for 24 h before being processed for a caspase 3 activity assay. *p* value denotes ANOVA with Bonferroni's multiple comparisons test.

For all panels, n=3 independent experiments and data are presented as the mean ± SD.

Figure 6. PITPα/β initiate the p53-PIP$_n$ signalosome by a PI binding-dependent mechanism

a, HEK293FT cells were co-transfected with either HA-tagged wild-type PITPα or PI binding-defective mutant T59D PITPα together with Flag-tagged p53^{wt}. After 48 h, cells were processed for IP against Flag-tag and analyzed by WB. *p* value denotes two-sided paired t-test.

b-d, MDA-MB-231 cells were transfected with control siRNAs or siRNAs against the 3'UTR of both PITPα and PITPβ for 24 h. Then, the cells were transfected with either HA-tagged wild-type PITPα/β or PI binding-defective mutant T59D PITPα/β. After 24 h, cells were treated with 30 μM cisplatin or vehicle for 24 h before being processed for WB (**b**) and IF staining against HA-tag with pAkt^{S473} (**c**). The nuclear pAkt^{S473} levels in HA-positive cells were quantified by ImageJ (**d**). n=3, 15 cells from each independent experiment. *p* value denotes two-sided paired t-test. Scale bar, 5 μm.

e-f, Pearson's correlation coefficient (Pearson's r) quantified the correlations between nuclear pAkt^{S473} and HA-PITPα$^{wt/T59D}$ levels. n=100 cells pooled from 3 independent experiments.

g-h, MDA-MB-231 cells were transfected with control siRNAs or siRNAs against the 3'UTR of both PITPα and PITPβ for 24 h. The cells were then transfected with either HA-tagged wild-type PITPα or PI binding-defective mutant T59D PITPα. After 24 h, cells were

treated with 30 μM cisplatin or vehicle for 24 h before being processed for Crystal Violet viability assay. The cells were imaged by an EVOS M5000 microscope (**g**) and quantified based on the extracted dye using a plate reader (**h**). *p* value denotes two-sided paired t-test. Scale bar, 300 μm.

i, MDA-MB-231 cells were transfected with control siRNAs or siRNAs against the 3'UTR of both PITPα and PITPβ for 24 h. The cells were then transfected with either HA-tagged wild-type PITPα or PI binding-defective mutant T59D PITPα. After 24 h, cells were treated with 30 μM cisplatin or vehicle for 24 h before being processed for a caspase 3 activity assay. *p* value denotes two-sided paired t-test.

j, A model of the stress-induced nuclear accumulation of class I PITPs and PITP-dependent initiation of the p53-PI signalosome, which promotes cell proliferation, survival, and invasion.

For all panels, n=3 independent experiments and data are presented as the mean ± SD.

Fig. 1

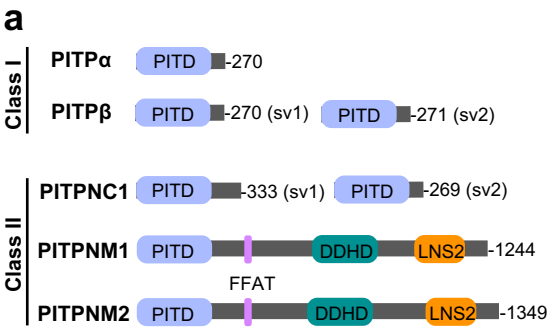

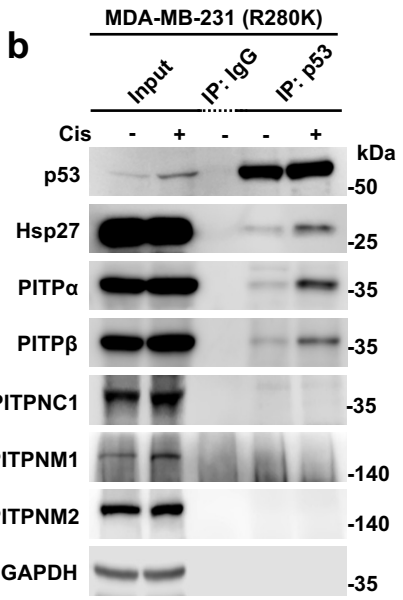

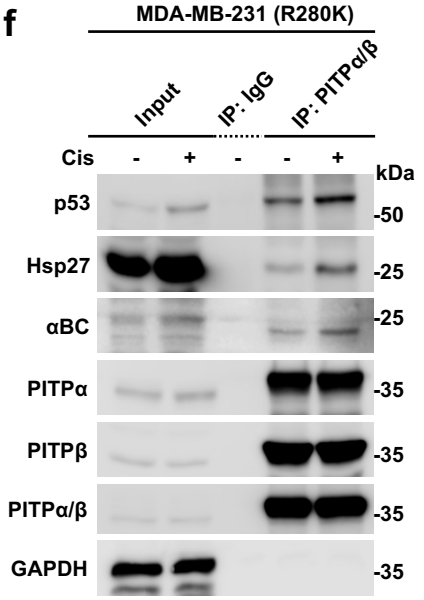

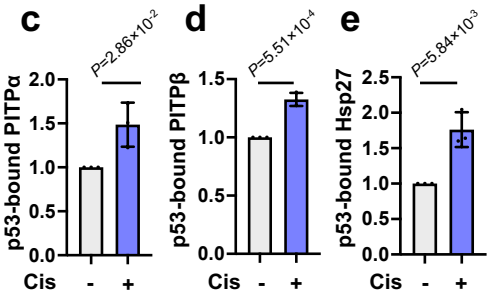

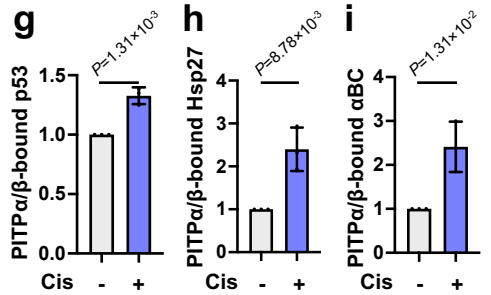

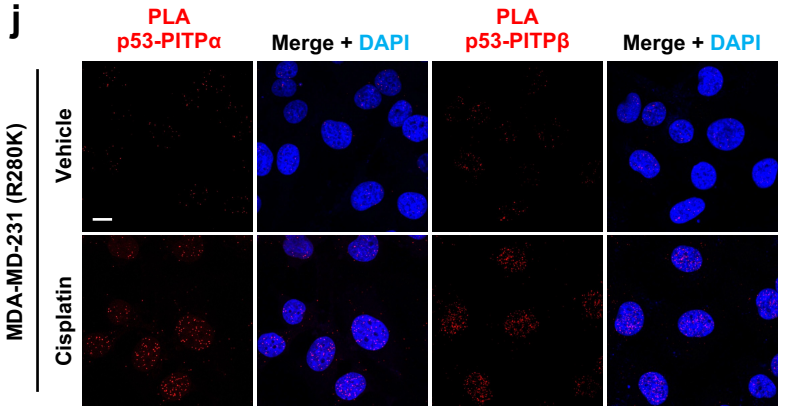

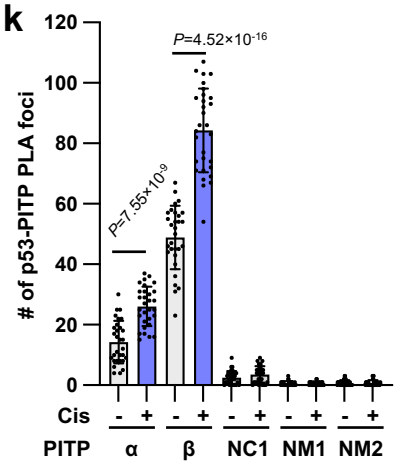

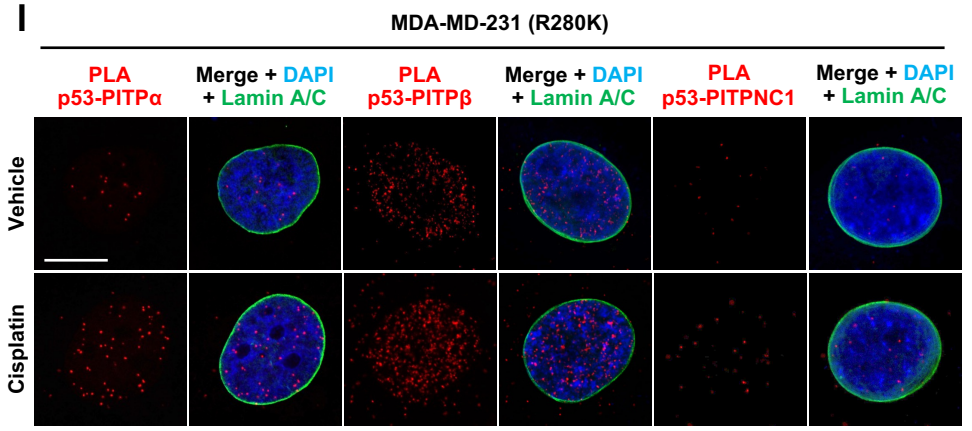

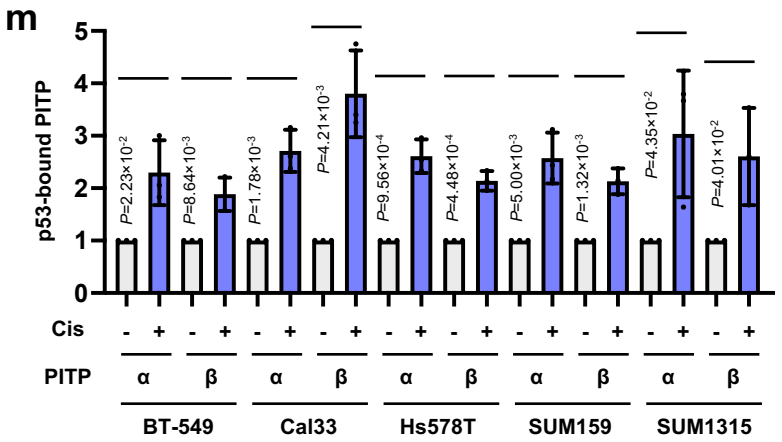

n

Microscale Thermophoresis (MST)	
Target Protein	Binding Affinity Kd with p53 (nM)
PITPα	1.23 ± 0.05
PITPα + PI (1μM)	15 ± 1
PITPβ	19 ± 2
PITPβ + PI (1μM)	5 ± 1
PITPNC1	NBD

Fig. 2

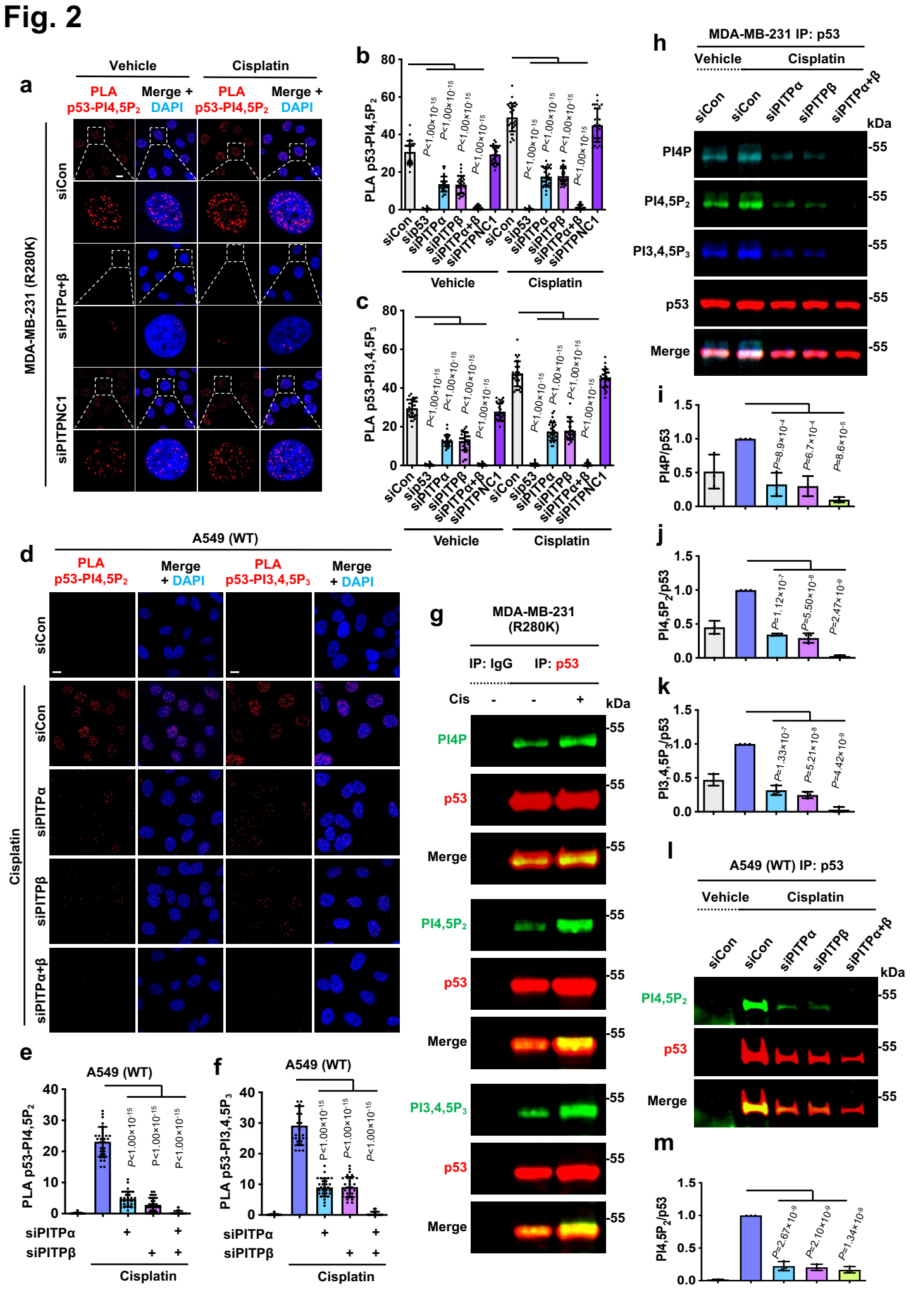
a
Vehicle
Cisplatin
PLA p53-PI4,5P2
Merge + DAPI
MDA-MB-231 (R280K)
siCon
siPITPα+β
siPITPNC1
b
PLA p53-PI4,5P2
siCon
sip53
siPITPα
siPITPβ
siPITPα+β
siPITPNC1
Vehicle
Cisplatin
c
PLA p53-PI3,4,5P3
d
A549 (WT)
PLA p53-PI4,5P2
Merge + DAPI
PLA p53-PI3,4,5P3
siPITPα
siPITPβ
e
A549 (WT)
PLA p53-PI4,5P2
siPITPα
siPITPβ
f
A549 (WT)
PLA p53-PI3,4,5P3
g
MDA-MB-231 (R280K)
IP: IgG
IP: p53
Cis
kDa
PI4P
p53
Merge
PI4,5P2
PI3,4,5P3
h
MDA-MB-231 IP: p53
PI4P
PI4,5P2
PI3,4,5P3
i
PI4P/p53
j
PI4,5P2/p53
k
PI3,4,5P3/p53
l
A549 (WT) IP: p53
m
PI4,5P2/p53

Fig. 3

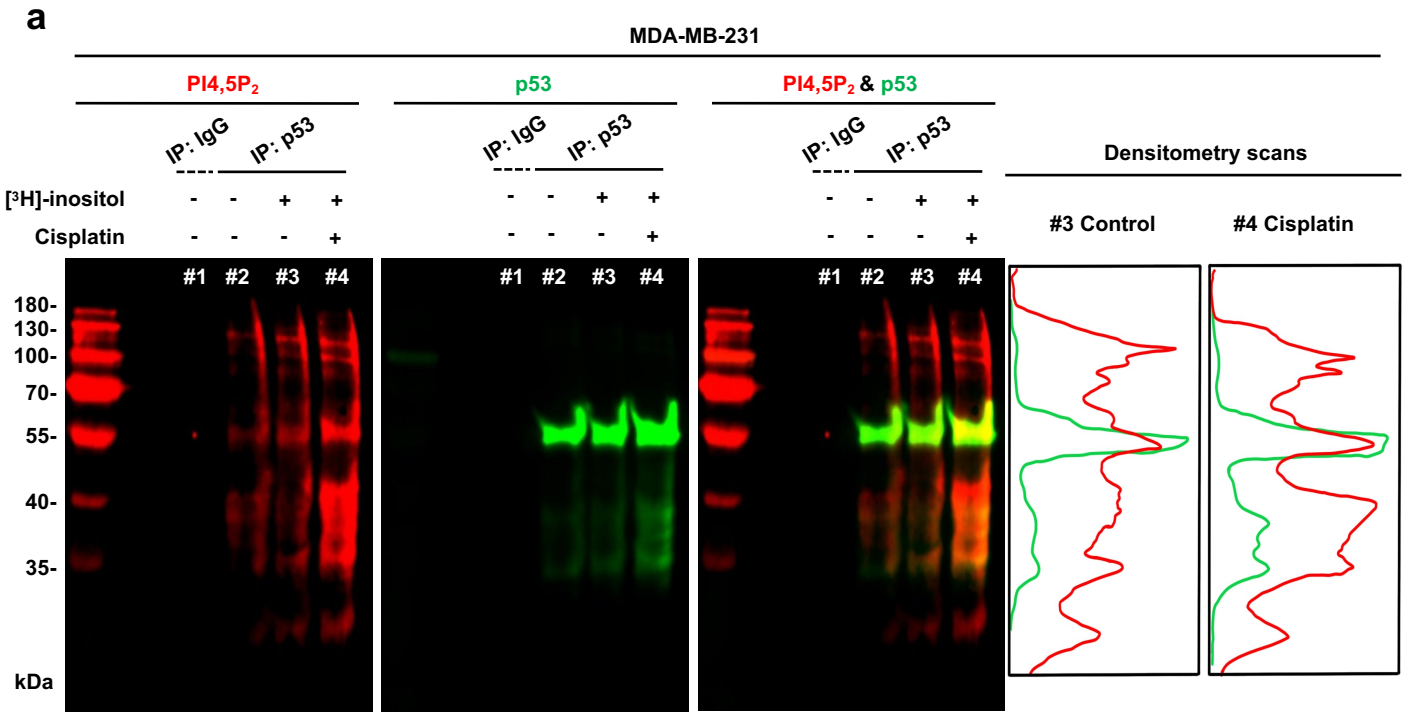
a
MDA-MB-231
PI4,5P2
p53
PI4,5P2 & p53
IP: IgG
IP: p53
[3H]-inositol
Cisplatin
#1 #2 #3 #4
180-
130-
100-
70-
55-
40-
35-
kDa
Densitometry scans
#3 Control
#4 Cisplatin

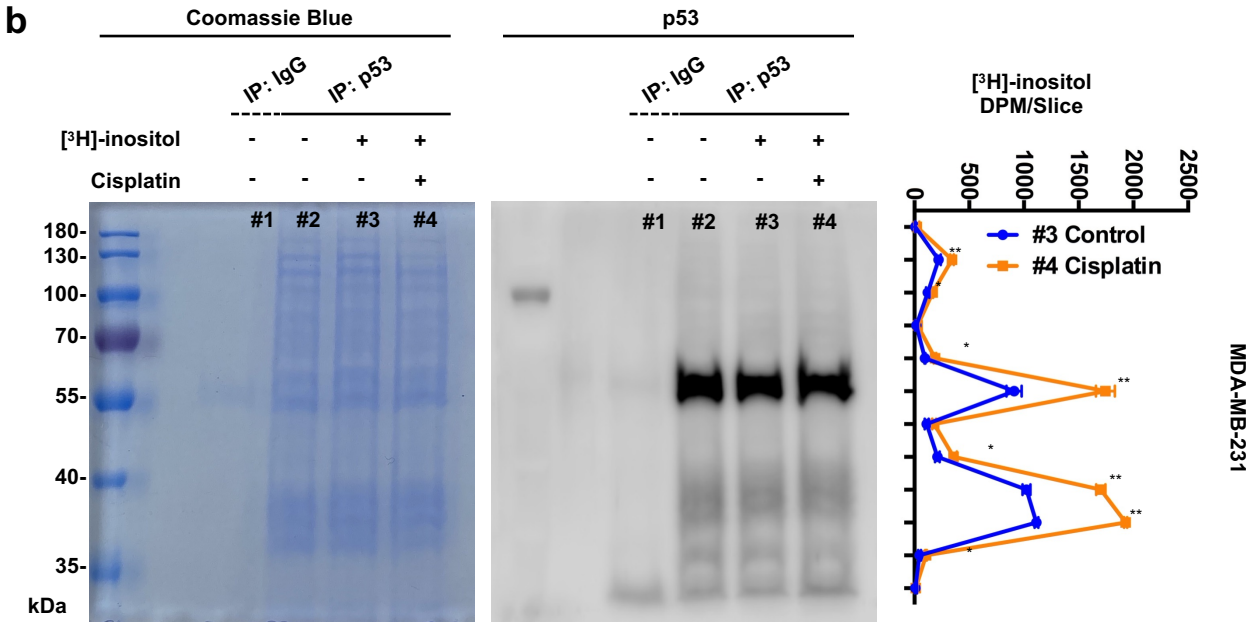
b
Coomassie Blue
p53
IP: IgG
IP: p53
[3H]-inositol
Cisplatin
#1 #2 #3 #4
180-
130-
100-
70-
55-
40-
35-
kDa
[3H]-inositol
DPM/Slice
0
500
1000
1500
2000
2500
#3 Control
#4 Cisplatin
MDA-MB-231

Fig. 4

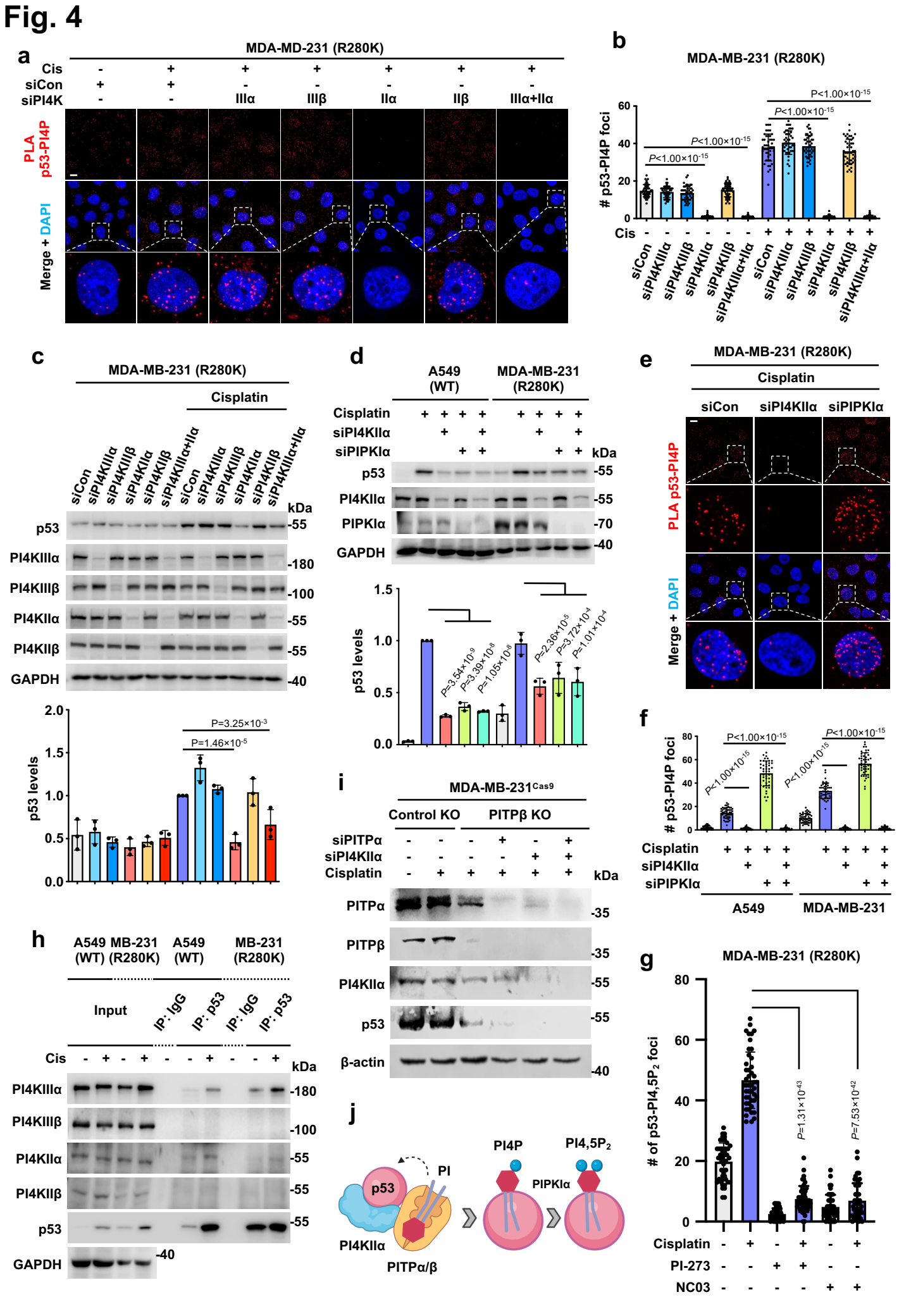
a
MDA-MD-231 (R280K)
Cis
siCon
siPI4K
IIIα
IIIβ
IIα
IIβ
IIIα+IIα
PLA p53-PI4P
Merge + DAPI
b
MDA-MB-231 (R280K)
p53-PI4P foci
P<1.00×10-15
Cis
siCon
siPI4KIIIα
siPI4KIIIβ
siPI4KIIα
siPI4KIIβ
siPI4KIIIα+IIα
c
MDA-MB-231 (R280K)
Cisplatin
kDa
p53
PI4KIIIα
PI4KIIIβ
PI4KIIα
PI4KIIβ
GAPDH
p53 levels
P=3.25×10-3
P=1.46×10-5
d
A549 (WT)
MDA-MB-231 (R280K)
Cisplatin
siPI4KIIα
siPIPKIα
p53
PI4KIIα
PIPKIα
GAPDH
p53 levels
P=3.54×10-9
P=3.39×10-8
P=1.05×10-8
P=2.36×10-5
P=3.72×10-4
P=1.01×10-4
e
MDA-MB-231 (R280K)
Cisplatin
siCon
siPI4KIIα
siPIPKIα
PLA p53-PI4P
Merge + DAPI
f
p53-PI4P foci
P<1.00×10-15
Cisplatin
siPI4KIIα
siPIPKIα
A549
MDA-MB-231
g
MDA-MB-231 (R280K)
# of p53-PI4,5P2 foci
P=1.31×10-43
P=7.53×10-42
Cisplatin
PI-273
NC03
h
A549 (WT)
MB-231 (R280K)
Input
IP: IgG
IP: p53
Cis
PI4KIIIα
PI4KIIIβ
PI4KIIα
PI4KIIβ
p53
GAPDH
i
MDA-MB-231Cas9
Control KO
PITPβ KO
siPITPα
siPI4KIIα
Cisplatin
PITPα
PITPβ
PI4KIIα
p53
β-actin
j
p53
PI
PI4KIIα
PITPα/β
PI4P
PIPKIα
PI4,5P2

Fig. 5

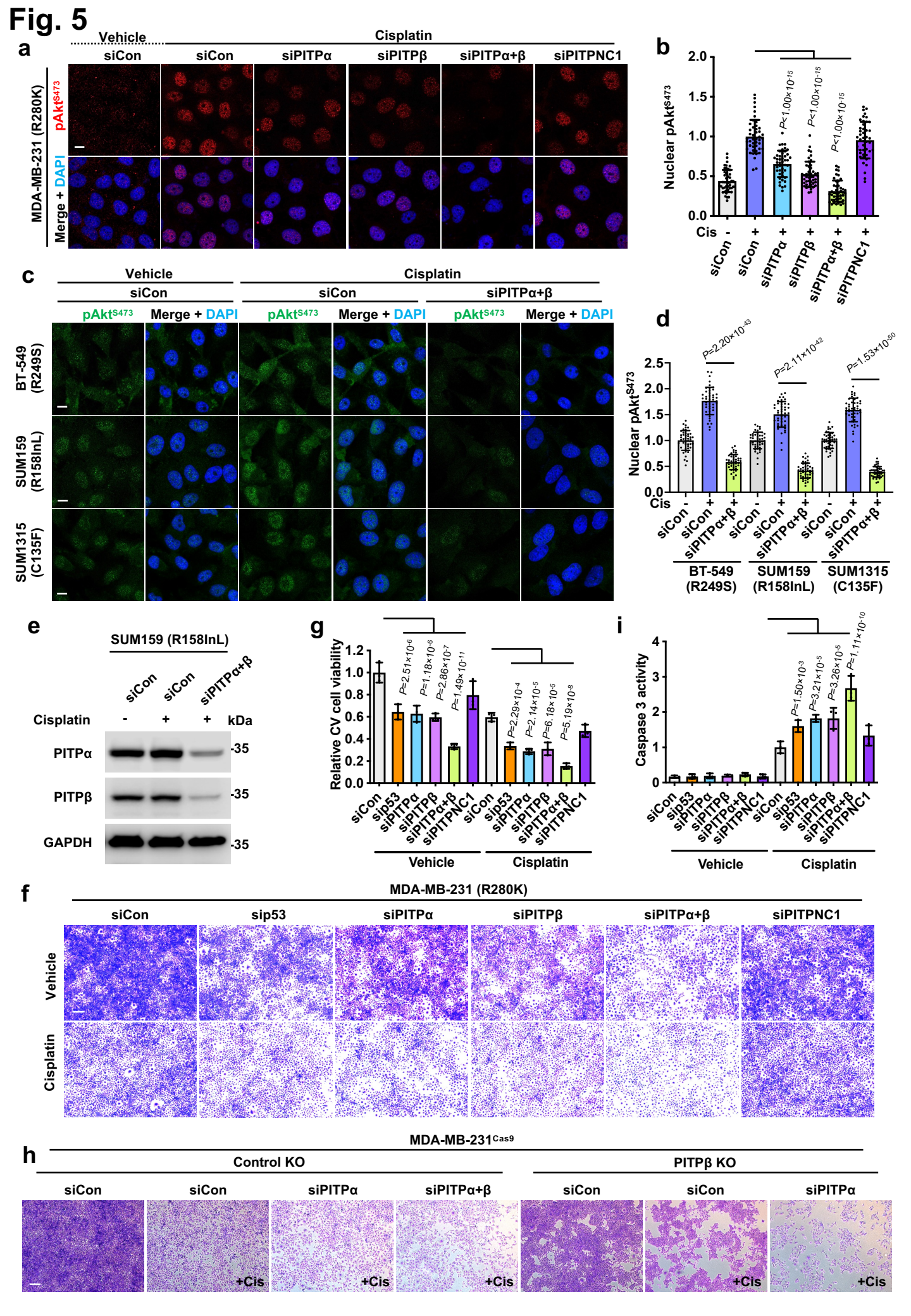
a
Vehicle
Cisplatin
siCon
siCon
siPITPα
siPITPβ
siPITPα+β
siPITPNC1
MDA-MB-231 (R280K)
pAktS473
Merge + DAPI
b
Nuclear pAktS473
2.0
1.5
1.0
0.5
0.0
P<1.00×10-15
P<1.00×10-15
P<1.00×10-15
Cis - + + + + +
siCon siCon siPITPα siPITPβ siPITPα+β siPITPNC1
c
Vehicle
Cisplatin
siCon
siCon
siPITPα+β
pAktS473
Merge + DAPI
BT-549 (R249S)
SUM159 (R158InL)
SUM1315 (C135F)
d
Nuclear pAktS473
P=2.20×10-43
P=2.11×10-42
P=1.53×10-50
Cis - + + - + + - + +
siCon siCon siPITPα+β siCon siCon siPITPα+β siCon siCon siPITPα+β
BT-549 (R249S)
SUM159 (R158InL)
SUM1315 (C135F)
e
SUM159 (R158InL)
siCon
siCon
siPITPα+β
Cisplatin - + +
kDa
PITPα
PITPβ
GAPDH
-35
-35
-35
g
Relative CV cell viability
P=2.51×10-6
P=1.18×10-6
P=2.86×10-7
P=1.49×10-11
P=2.29×10-4
P=2.14×10-5
P=6.18×10-5
P=5.19×10-8
siCon sip53 siPITPα siPITPβ siPITPα+β siPITPNC1 siCon sip53 siPITPα siPITPβ siPITPα+β siPITPNC1
Vehicle
Cisplatin
i
Caspase 3 activity
P=1.50×10-3
P=3.21×10-5
P=3.26×10-5
P=1.11×10-10
siCon sip53 siPITPα siPITPβ siPITPα+β siPITPNC1 siCon sip53 siPITPα siPITPβ siPITPα+β siPITPNC1
Vehicle
Cisplatin
f
MDA-MB-231 (R280K)
siCon
sip53
siPITPα
siPITPβ
siPITPα+β
siPITPNC1
Vehicle
Cisplatin
h
MDA-MB-231Cas9
Control KO
PITPβ KO
siCon
siCon
siPITPα
siPITPα+β
siCon
siCon
siPITPα
+Cis
+Cis
+Cis
+Cis
+Cis
+Cis

Fig. 6

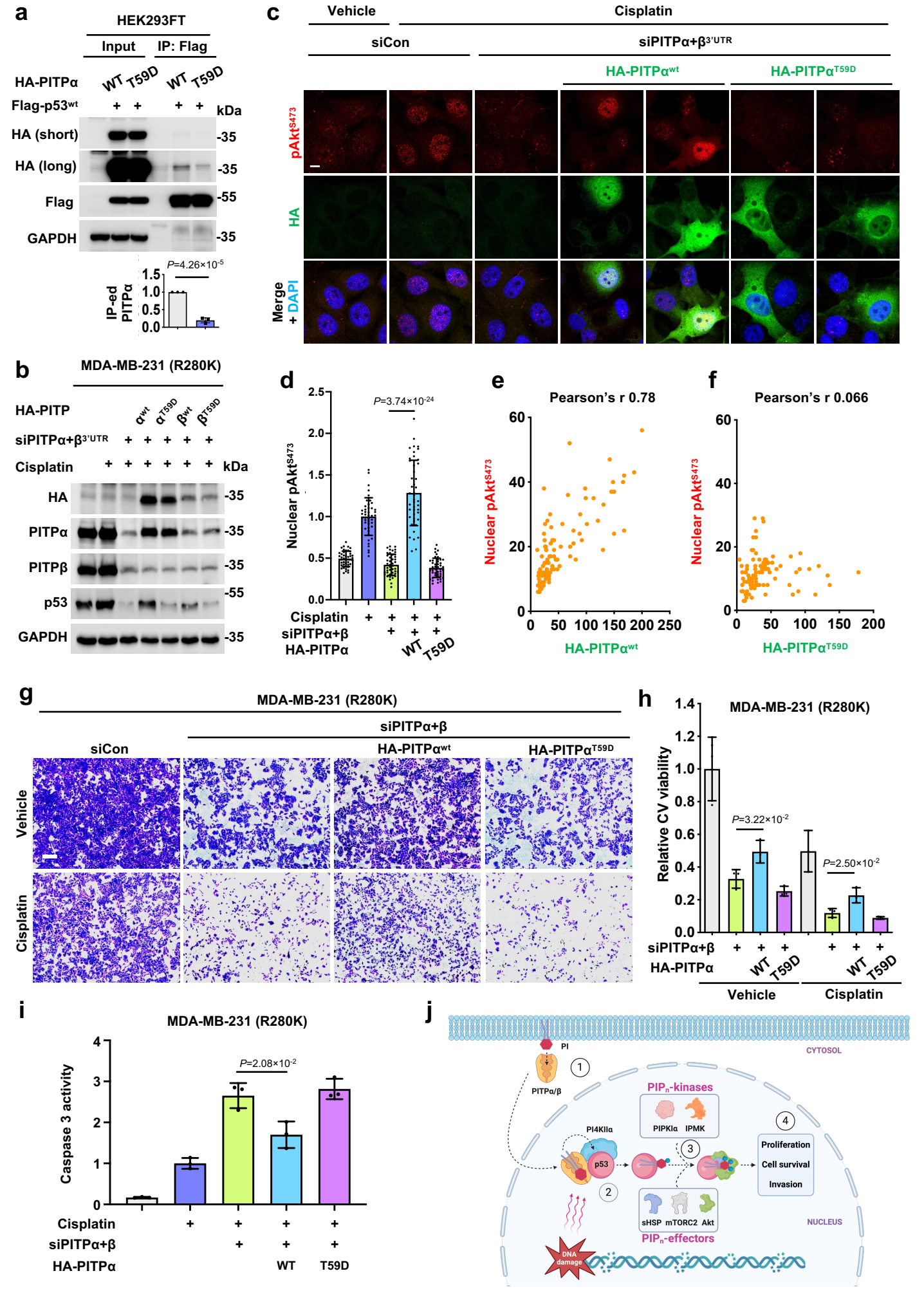
a
HEK293FT
Input
IP: Flag
HA-PITPα
WT T59D WT T59D
Flag-p53wt
+ + + +
kDa
HA (short)
HA (long)
Flag
GAPDH
-35
-35
-55
-35
P=4.26×10-5
IP-ed PITPα
1.5
1.0
0.5
0.0
b
MDA-MB-231 (R280K)
HA-PITP
αwt αT59D βwt βT59D
siPITPα+β3'UTR
Cisplatin
HA
PITPα
PITPβ
p53
GAPDH
c
Vehicle
Cisplatin
siCon
siPITPα+β3'UTR
HA-PITPαwt
HA-PITPαT59D
pAktS473
HA
Merge + DAPI
d
P=3.74×10-24
Nuclear pAktS473
Cisplatin
siPITPα+β
HA-PITPα
WT T59D
e
Pearson's r 0.78
Nuclear pAktS473
HA-PITPαwt
f
Pearson's r 0.066
Nuclear pAktS473
HA-PITPαT59D
g
MDA-MB-231 (R280K)
siPITPα+β
siCon
HA-PITPαwt
HA-PITPαT59D
Vehicle
Cisplatin
h
MDA-MB-231 (R280K)
Relative CV viability
P=3.22×10-2
P=2.50×10-2
siPITPα+β
HA-PITPα
WT T59D WT T59D
Vehicle
Cisplatin
i
MDA-MB-231 (R280K)
Caspase 3 activity
P=2.08×10-2
Cisplatin
siPITPα+β
HA-PITPα
WT T59D
j
PI
PITPα/β
CYTOSOL
PIPn-kinases
PIPKIα IPMK
PI4KIIα
p53
Proliferation
Cell survival
Invasion
sHSP mTORC2 Akt
PIPn-effectors
NUCLEUS
DNA damage

Extended Data Fig. 1

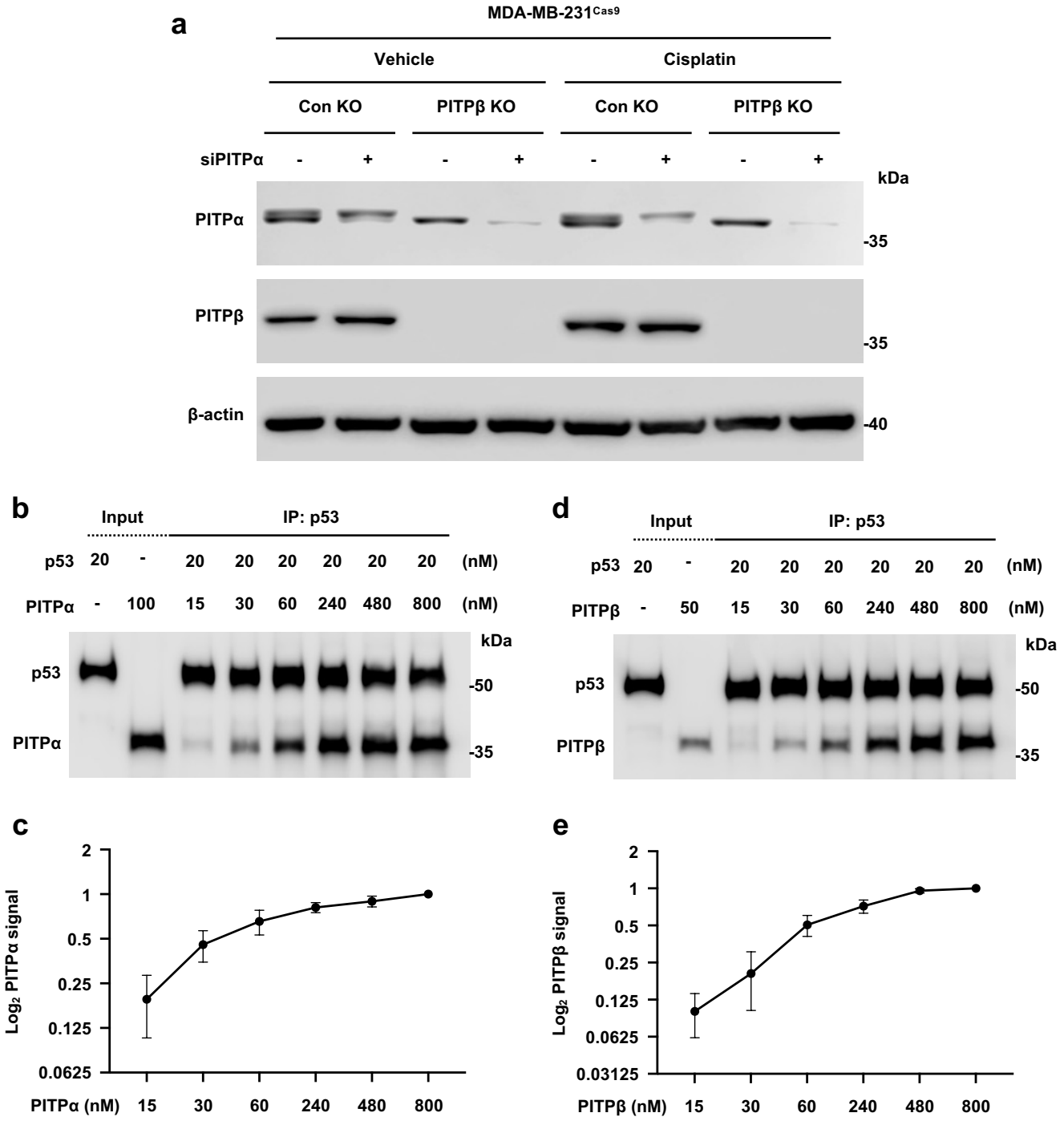

Extended Data Figure 1. PITPα/β validation and interaction with p53

a, MDA-MB-231^{Cas9} cells with PITPβ KO and control non-targeted KO were transfected with control siRNAs or siRNAs against PITPα. After 48 h, cells were processed for WB to analyze PITPα and PITPβ expression. n=3 independent experiments.

b-e, *In vitro* binding of recombinant p53 and PITPα (**b-c**) and p53 and PITPβ (**d-e**). Anti-p53 antibody-conjugated agarose was incubated with constant p53 and increasing PITPα or PITPβ protein. p53 was then IPed and analyzed by WB and quantified by ImageJ for p53-bound PITPα (**c**) and p53-bound PITPβ (**e**). n=3 independent experiments.

For all graphs, data are presented as the mean ± SD.

Extended Data Fig. 2

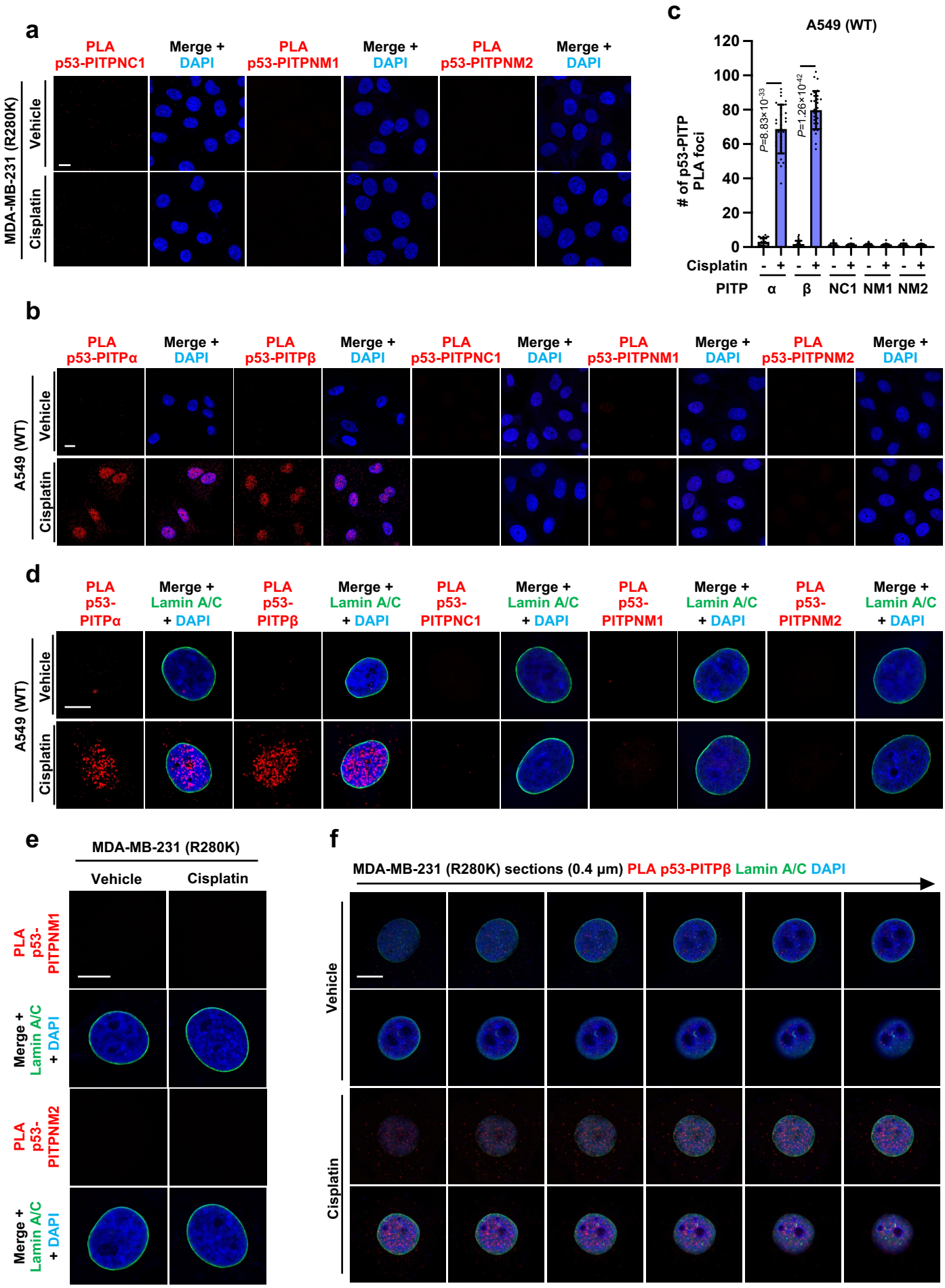

Extended Data Figure 2. p53 interacts with class I PITPs in the nucleus in response to stress

a, PLA of p53-PITPα/PITPβ/PITPNC1/PITPNM1/PITPNM2 in MDA-MB-231 cells treated with vehicle or 30 μM cisplatin for 24 h. n=3, 10 cells from each independent experiment. *p* value denotes two-sided paired t-test. See expanded images in Fig. 1j and quantification in Fig. 1k.

b-c, PLA of p53-PITPα/PITPβ/PITPNC1/PITPNM1/PITPNM2 in A549 cells treated with vehicle or 30 μM cisplatin for 24 h. The nuclear p53-PITP foci were quantified (**c**). n=3, 10 cells from each independent experiment. *p* value denotes two-sided paired t-test.

d, PLA of p53-PITPα/PITPβ/PITPNC1/PITPNM1/PITPNM2 overlaid with the nuclear envelope marker Lamin A/C in A549 cells treated with vehicle or 30 μM cisplatin for 24 h. The nuclei were counterstained by DAPI. n=3 independent experiments.

e, PLA of p53-PITPα/PITPβ/PITPNC1/PITPNM1/PITPNM2 overlaid with the nuclear envelope marker Lamin A/C in MDA-MB-231 cells treated with vehicle or 30 μM cisplatin for 24 h. The nuclei were counterstained by DAPI. n=3 independent experiments. See expanded images in Fig. 1l.

f, 3D sections of p53-PITPβ PLA foci overlaid with Lamin A/C in MDA-MB-231 treated with vehicle or 30 μM cisplatin for 24 h. The nuclei were counterstained by DAPI. Each frame of the 3D sections was over a 0.2 μm thickness.

For all graphs, data are presented as the mean ± SD. Scale bar, 5 μm.

Extended Data Fig. 3

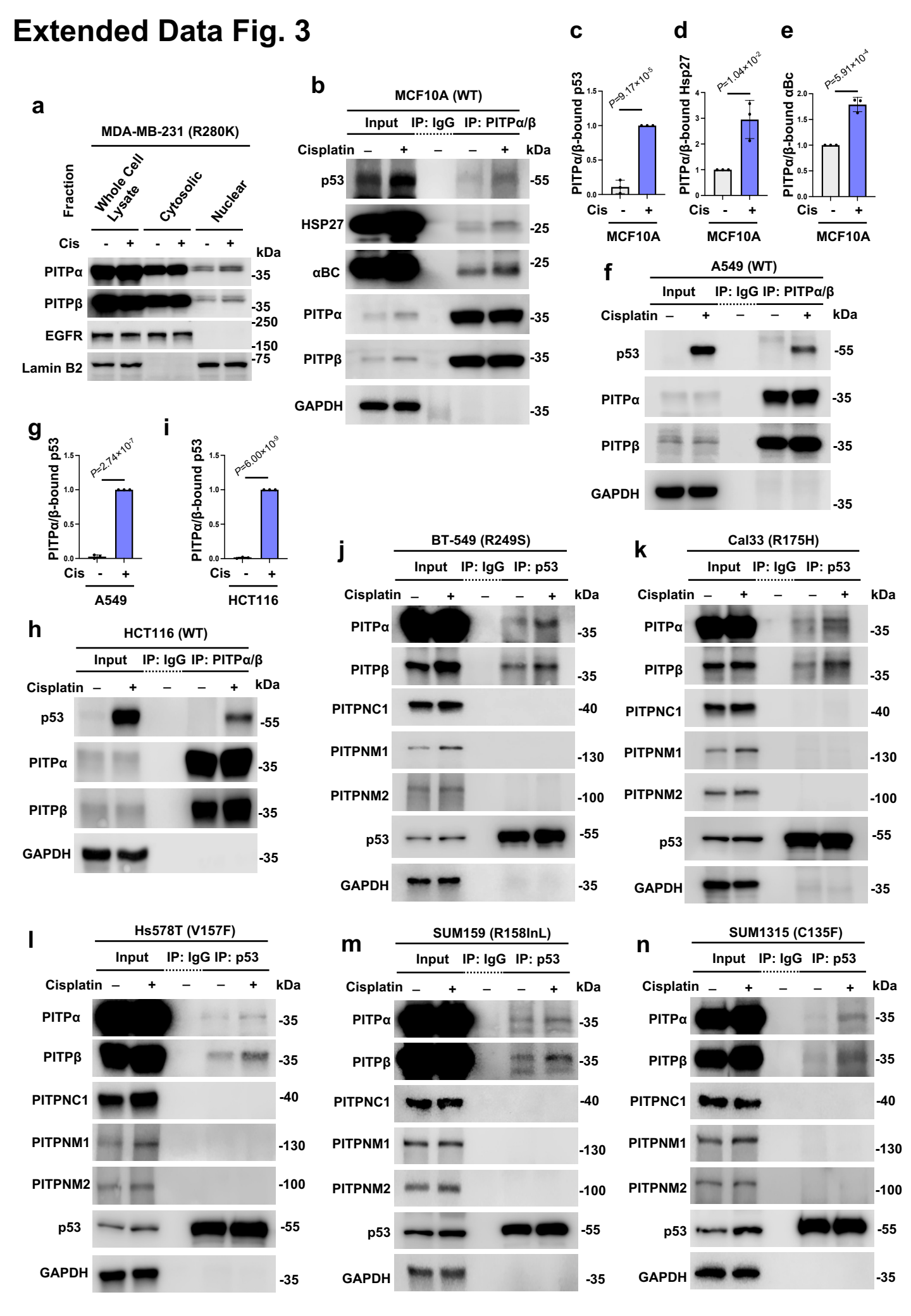

Extended Data Figure 3. p53 interacts with class I PITPs in multiple cell lines

a, MDA-MB-231 cells were treated with vehicle or cisplatin for 24 h. Cells were then fractionated using a detergent-based extraction to produce lysates from cytosolic and nuclear fractions and analyzed via WB. n=3 independent experiments.

b-e, Co-IP of p53/Hsp27/αB-crystallin (αBC) with the shared epitope of PITPα/β in MCF10A cells treated with vehicle or 30 μM cisplatin for 24 h. p53 immunoprecipitated (IPed) by PITPα/β (**c**), Hsp27 IPed by PITPα/β (**d**), and αBC IPed by PITPα/β (**e**) were analyzed by WB. n=3 independent experiments.

f-g, Co-IP of p53 with the shared epitope of PITPα/β in A549 cells treated with vehicle or 30 μM cisplatin for 24 h. p53 IPed by PITPα/β was analyzed by WB (**g**). n=3 independent experiments.

h-i, Co-IP of p53 with the shared epitope of PITPα/β in HCT116 cells treated with vehicle or 30 μM cisplatin for 24 h. p53 IPed by PITPα/β was analyzed by WB (**i**). n=3 independent experiments.

j-n, Co-IP of PITPα/PITPβ with p53 in BT549, Cal33, HS578T, SUM159, SUM1315 cells treated with vehicle or 30 μM cisplatin for 24 h. PITPα/PITPβ IPed by p53 and PITPNC1/PITPNM1/PITPNM2 were analyzed by WB. n=3 independent experiments.

For all panels, data are represented as mean ± SD, and the *p* value denotes a two-sided paired t-test.

Extended Data Fig. 4

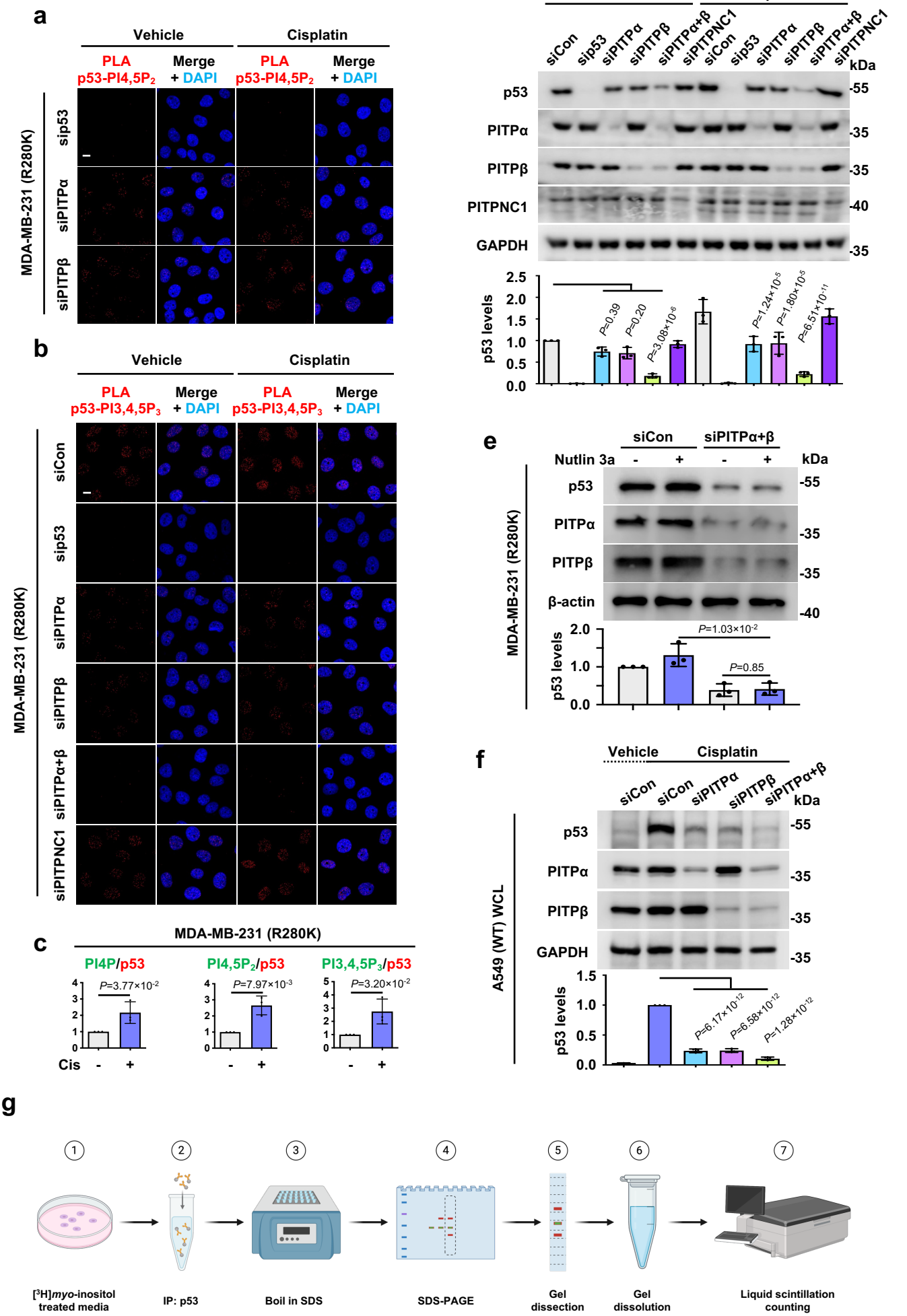

Extended Data Figure 4. PITPα/β regulate p53-PIP_n complexes and p53 levels

a-b, MDA-MB-231 cells were transfected with control siRNAs or siRNAs against p53, PITPα, PITPβ, PITPNC1, or both PITPα and PITPβ. After 24 h, cells were treated with 30 μM cisplatin or vehicle for 24 h before being processed for PLA to detect p53-PI4,5P_2 (**a**) and p53-PI3,4,5P_3 (**b**) complexes. n=3 independent experiments. See KD validation in Extended Data Fig. 4d, expanded images in Fig. 2a, and quantification in Fig. 2b,c.

c, MDA-MB-231 cells were treated with 30 μM cisplatin or vehicle for 24 h before being processed for IP against p53. p53-bound PI4P/PI4,5P_2/PI3,4,5P_3 were examined by fluorescent WB in Fig. 2g before being analyzed by imageJ. n=3 independent experiments. *p* value denotes two-sided paired t-test.

d, MDA-MB-231 cells were transfected with control siRNAs or siRNAs against p53, PITPα, PITPβ, PITPNC1, or both PITPα and PITPβ. After 24 h, cells were treated with 30 μM cisplatin or vehicle for 24 h before being processed for WB to validate the KD. The p53 level was quantified by ImageJ. n=3 independent experiments. *p* value denotes ANOVA with Bonferroni's multiple comparisons test.

e, MDA-MB-231 cells were transfected with control siRNAs or siRNAs against both PITPα and PITPβ. After 24 h, cells were treated with 10 μM Nutlin 3a or vehicle for 24 h before being processed for WB and analyzed using ImageJ. *p* value denotes two-sided paired t-test. n=3 independent experiments.

f, A549 cells were transfected with control siRNAs or siRNAs against PITPα, PITPβ, or both PITPα and PITPβ. After 24 h, cells were treated with 30 μM cisplatin or vehicle for 24 h before being processed for WB. The p53 level was quantified by ImageJ. n=3 independent experiments. *p* value denotes ANOVA with Bonferroni's multiple comparisons test.

g, A model of the [^{3}H]-inositol lableing workflow used to detect p53-PIP_n complexes. See related data in Fig. 3a-b.

For all panels, data are represented as mean ± SD. Scale bar, 5 μm.

Extended Data Fig. 5

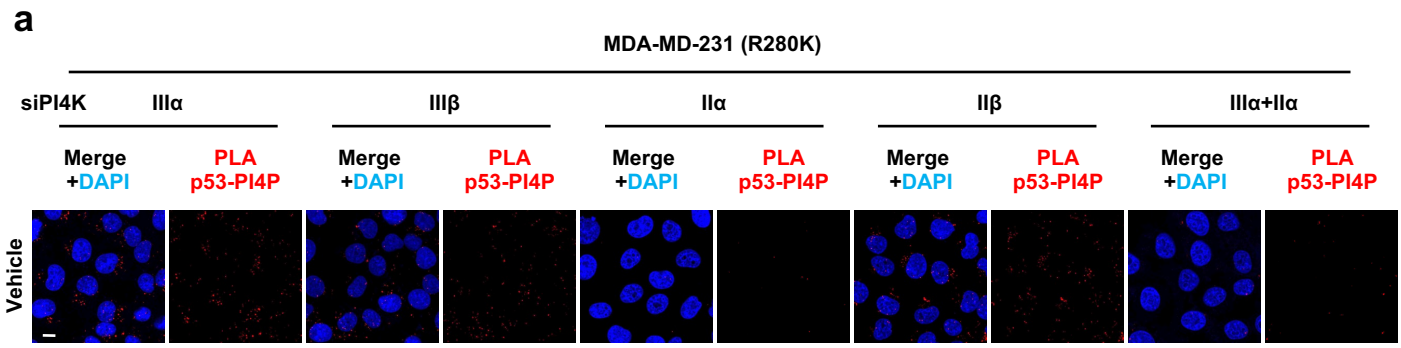

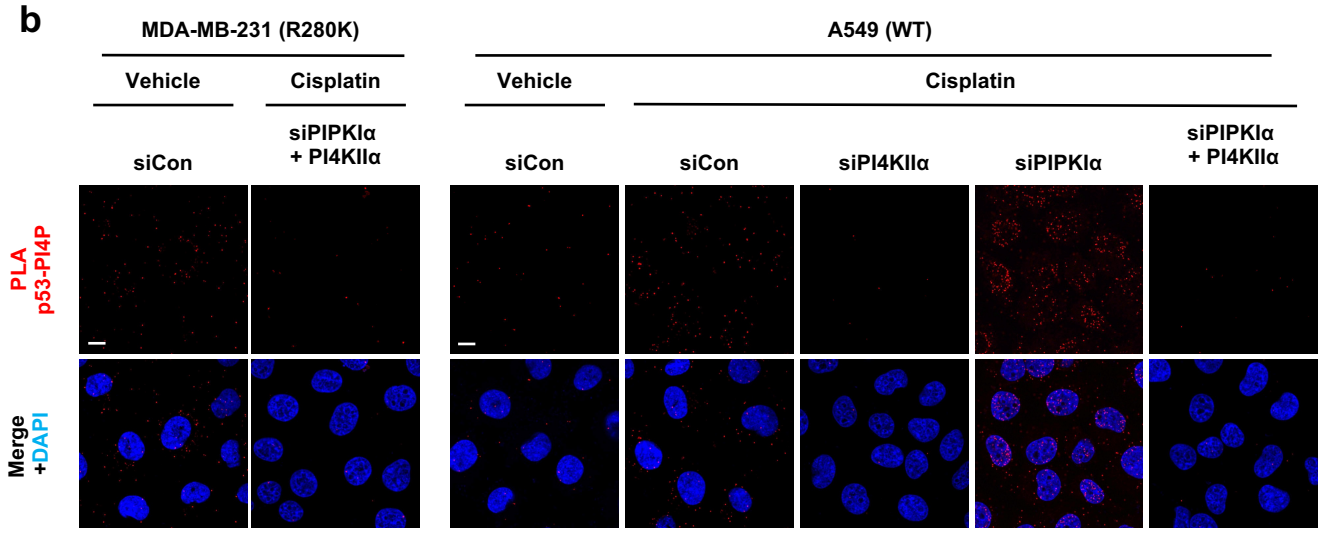

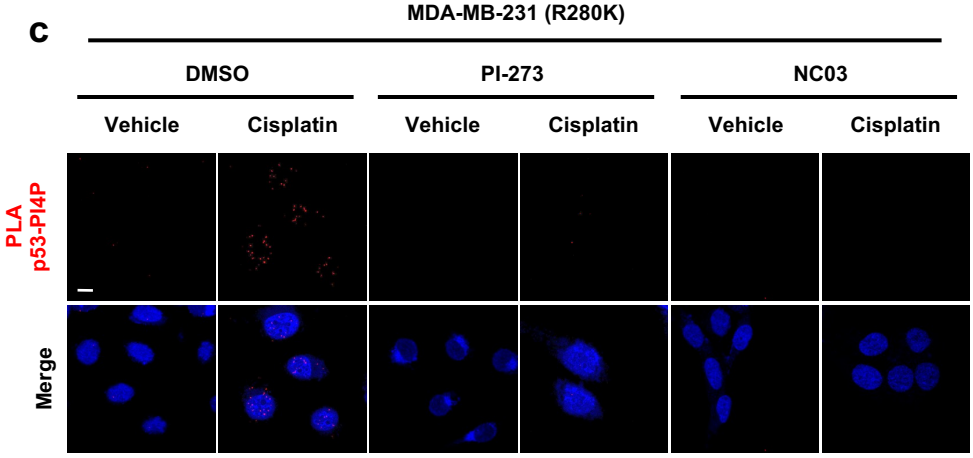

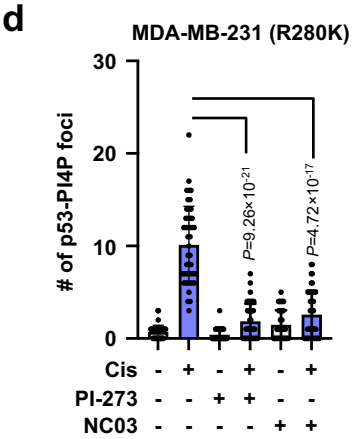

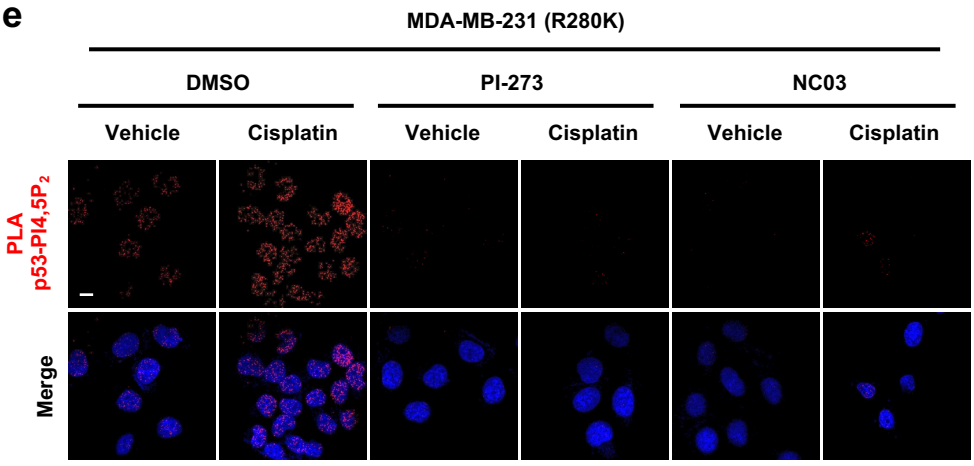

Extended Data Figure 5. PI4KIIα activity is required to generate p53-PI4P

a, MDA-MB-231 cells were transfected with control siRNAs or siRNAs against PI4KIIIα, PI4KIIIβ, PI4KIIα, PI4KIIβ or both PI4KIIα and PI4KIIIα. After 24 h, cells were treated with 30 μM cisplatin or vehicle for 24 h before being processed for PLA to detect p53-PI4P complexes (**b**). n=3 independent experiment. See expanded images in Fig. 4a and quantification in Fig. 4b.

b, MDA-MB-231 and A549 cells were transfected with control siRNAs or siRNAs against PI4KIIIα, PIPKIα or both PI4KIIα and PIPKIα. After 24 h, cells were treated with 30 μM cisplatin or vehicle for 24 h before being processed for PLA to detect p53-PI4P complexes. n=3 independent experiment. See KD confirmation in Fig. 4d, expanded images in Fig. 4e, and quantification in Fig. 4f.

c-d, MDA-MB-231 cells were treated with vehicle or cisplatin in combination with DMSO as a control, PI-273, or NC03 for 24 h before being processed for PLA to detect p53-PI4P complexes and analyzed using ImageJ (**d**). *p* value denotes two-sided paired t-test. n=3, 15 cells from each independent experiment.

e, MDA-MB-231 cells were treated with vehicle or cisplatin in combination with DMSO as a control, PI-273, or NC03 for 24 h before being processed for PLA to detect p53-PI4,5P_2 complexes. n=3 independent experiments. See quantification in Fig. 4g.

For all panels, scale bar, 5 μm.

Extended Data Fig. 6

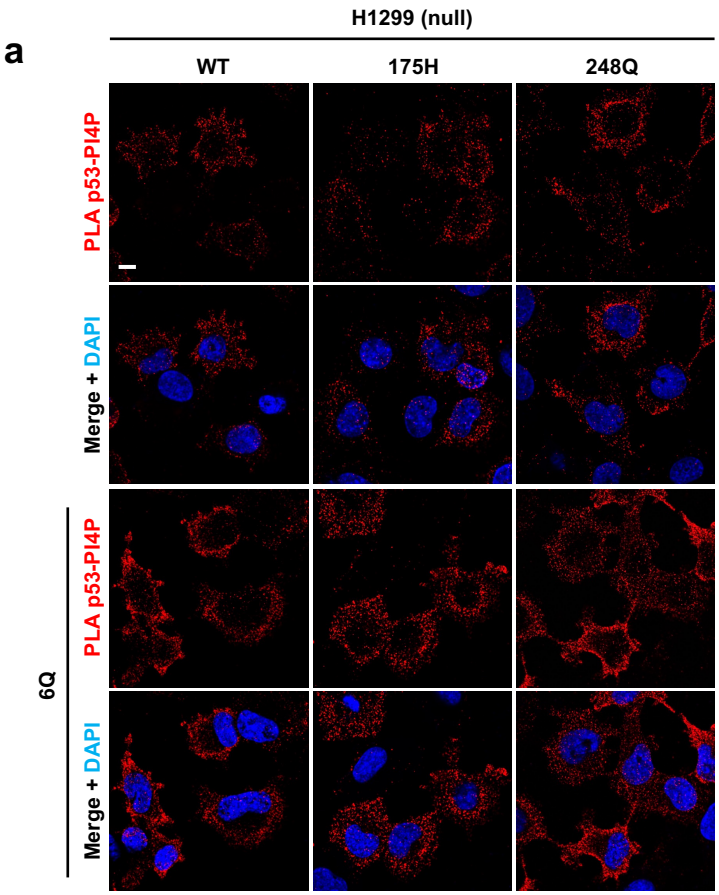

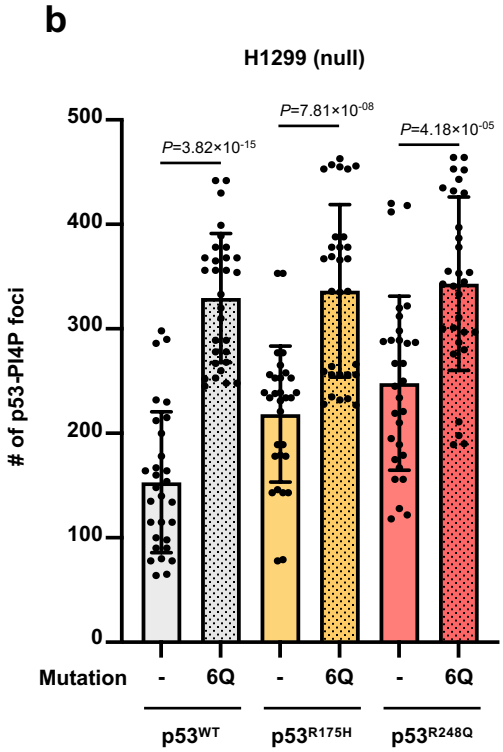

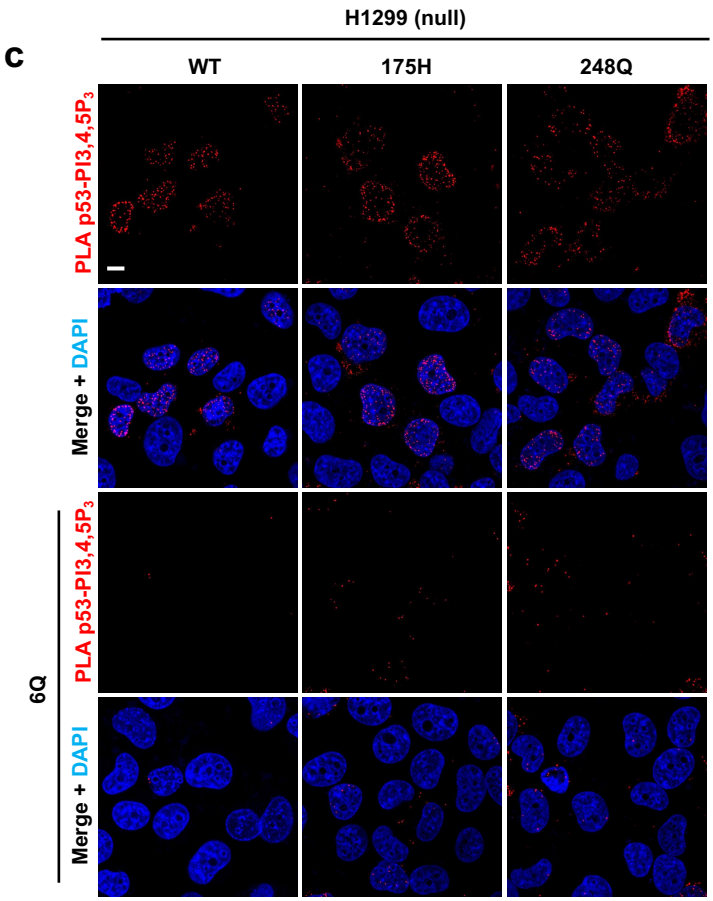

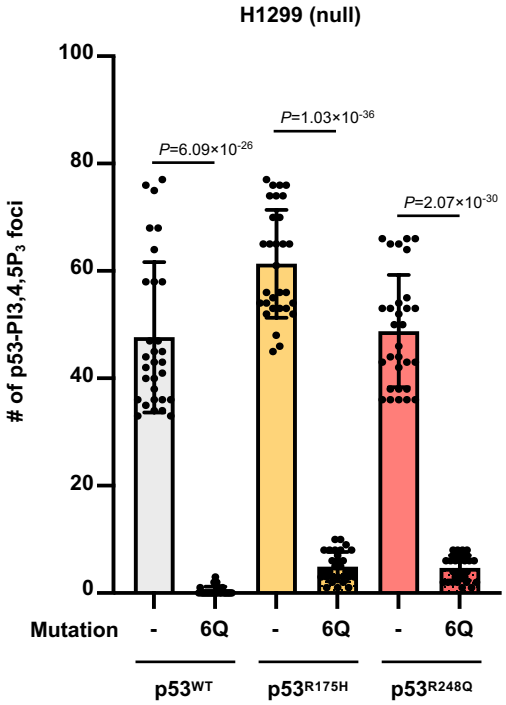

Extended Data Figure 6. p53^{6Q} mutants still form p53-PI4P complexes

a-b, H1299 cells transfected with constructs expressing p53 WT, WT6Q, 175H, 175H6Q, 248Q and 248Q6Q were treated with 30 μM cisplatin for 24 h. Then, the cells were processed for PLA to detect p53-PI4P complexes (**b**). Nuclei were counterstained by DAPI. *p* value denotes two-sided paired t-test. n=3 independent experiments.

c-d, H1299 cells transfected with constructs expressing p53 WT, WT6Q, 175H, 175H6Q, 248Q, and 248Q6Q were treated with 30 μM cisplatin for 24 h. Then, the cells were processed for PLA to detect p53-PI3,4,5P_3 complexes (**d**). Nuclei were counterstained by DAPI. *p* value denotes two-sided paired t-test. n=3 independent experiments.

For all panels, data are represented as mean ± SD. Scale bar, 5 μm.

Extended Data Fig. 7

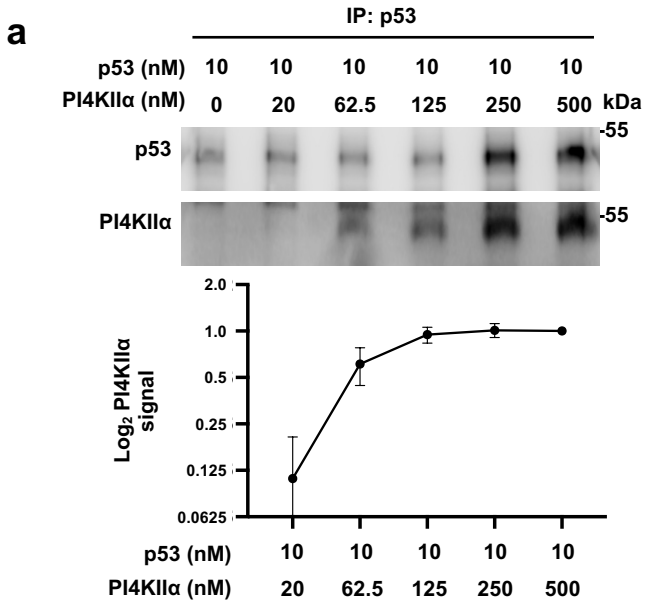

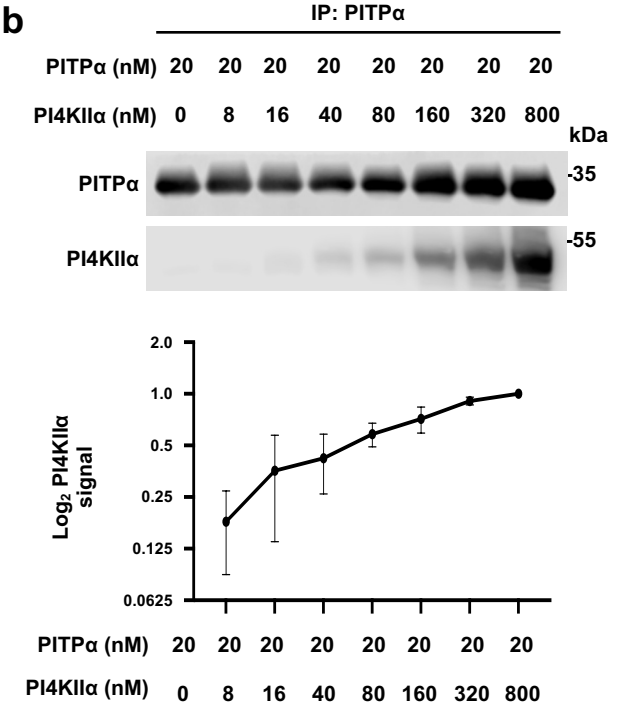

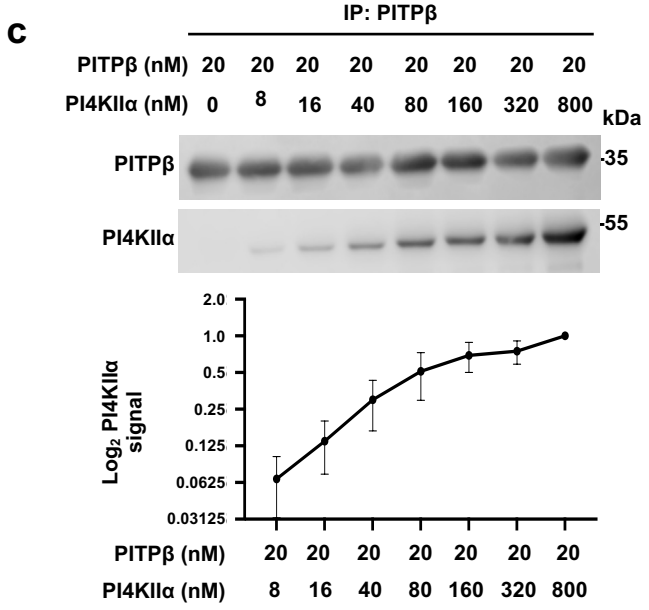

d

Microscale Thermophoresis (MST)	
Target Protein	Binding Affinity Kd with PI4KIIα (nM)
p53	8 ± 1
PITPα	189 ± 26
PITPα + PI (1μM)	16 ± 2
PITPβ	263 ± 12
PITPβ + PI (1μM)	113 ± 11

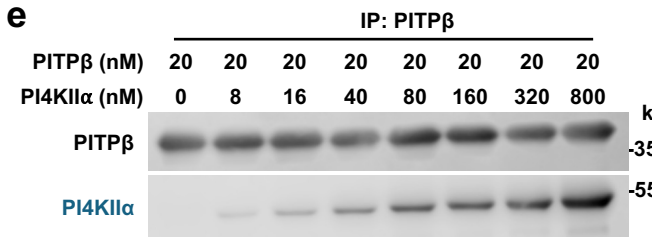

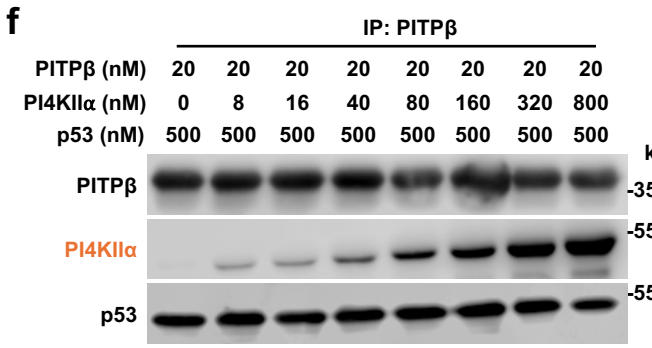

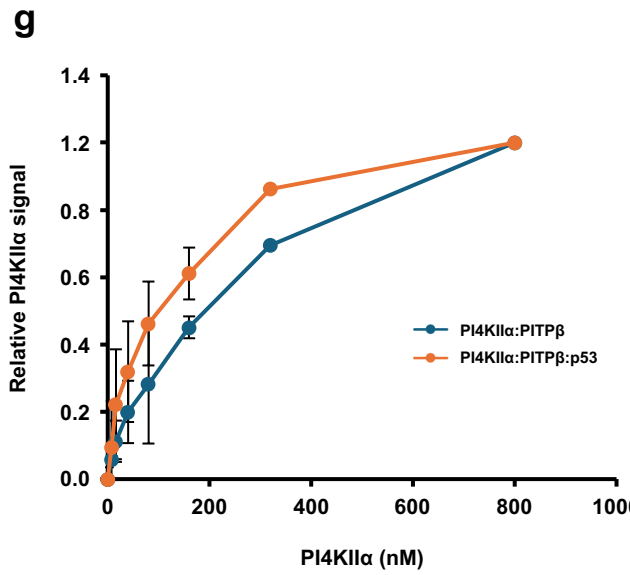

Extended Data Figure 7. PI4KIIα interacts with PITPα/β and p53 cooperatively

a-c, *In vitro* binding of recombinant PI4KIIα and p53 (**a**), PI4KIIα and PITPα (**b**), and PI4KIIα and PITPβ (**c**). p53, PITPα, or PITPβ immobilized on the indicated antibody-conjugated agarose was incubated with PI4KIIα protein. p53, PITPα or PITPβ was IPed and p53-bound PI4KIIα (**a**), PITPα-bound PI4KIIα (**b**) and PITPβ-bound PI4KIIα (**c**) was analyzed by WB and quantified by ImageJ. n=3 independent experiments.

d, The interaction of recombinant fluorescently labelled PI4KIIα with other components was quantitated by MST assay. A constant concentration of fluorescently labelled PI4KIIα (5 nM) was incubated with increasing concentrations of non-labelled ligand with or without the addition of 1 μM PI and analyzed using a Monolith NT.115 pico, and the binding affinity was autogenerated by MO. Control v.1.6 software. The binding affinities determined by MST are shown as indicated K_d values. n=3 independent experiments.

e-g, *In vitro* binding of recombinant PITPβ and PI4KIIα with and without p53. Anti-PITPβ antibody-conjugated agarose was incubated with constant PITPβ and increasing PI4KIIα protein in the absence (**e**) or presence (**f**) of p53. PITPβ was then IPed, analyzed by WB, and quantified by ImageJ for PITPβ-bound PI4KIIα. n=3 independent experiments.

For all panels, data are presented as the mean ± SD.

Extended Data Fig. 8

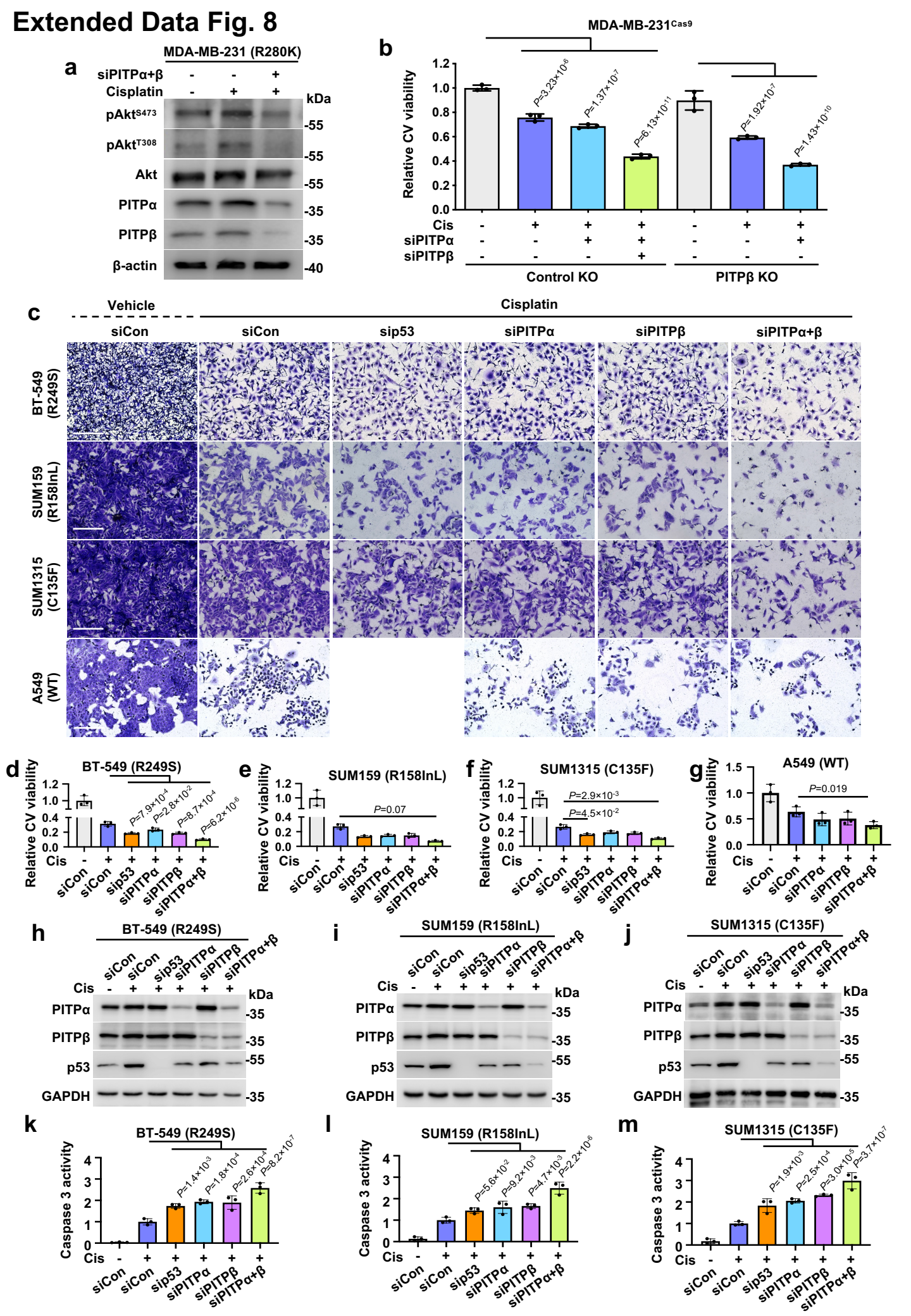

Extended Data Figure 8. PITPα/β regulate Akt activation and chemoresistance

a, MDA-MB-231 cells were transfected with control siRNAs or siRNAs against both PITPα and PITPβ. After 24 h, cells were treated with 30 μM cisplatin or vehicle for 24 h before being processed for WB. n=3 independent experiments.

b, MDA-MB-231^{Cas9} cells with PITPβ KO and control non-targeted KO were transfected with control siRNAs or siRNAs against PITPα, PITPβ, or both PITPα and PITPβ. After 24 h, cells were treated with 30 μM cisplatin or vehicle for 24 h before being processed for Crystal Violet viability assay. Viability was quantified based on the extracted dye using a plate reader. *p* value denotes ANOVA with Bonferroni's multiple comparisons test. n=3 independent experiments. See representative images in Fig. 5h.

c-j, BT-549, SUM159, and SUM1315 cells were transfected with control siRNAs or siRNAs against p53, PITPα, PITPβ, or both PITPα and PITPβ. A549 cells were transfected with control siRNAs or siRNAs against PITPα, PITPβ, or both PITPα and PITPβ. After 24 h, cells were treated with 30 μM cisplatin or vehicle for 24 h before being processed for Crystal Violet viability assay. The cells were imaged by an EVOS M5000 microscope (**c**) and quantified based on the extracted dye using a plate reader (**d-f**). The KD was validated by WB (**g-i**). *p* value denotes ANOVA with Bonferroni's multiple comparisons test. n=3 independent experiments.

k-m, BT-549, SUM159, and SUM1315 cells were transfected with control siRNAs or siRNAs against p53, PITPα, PITPβ, or both PITPα and PITPβ. After 24 h, cells were treated with 30 μM cisplatin or vehicle for 24 h before being processed for a caspase 3 activity assay. *p* value denotes ANOVA with Bonferroni's multiple comparisons test. n=3 independent experiments.

For all graphs, data are presented as the mean ± SD. Scale bar, 300 μm.

Extended Data Fig. 9

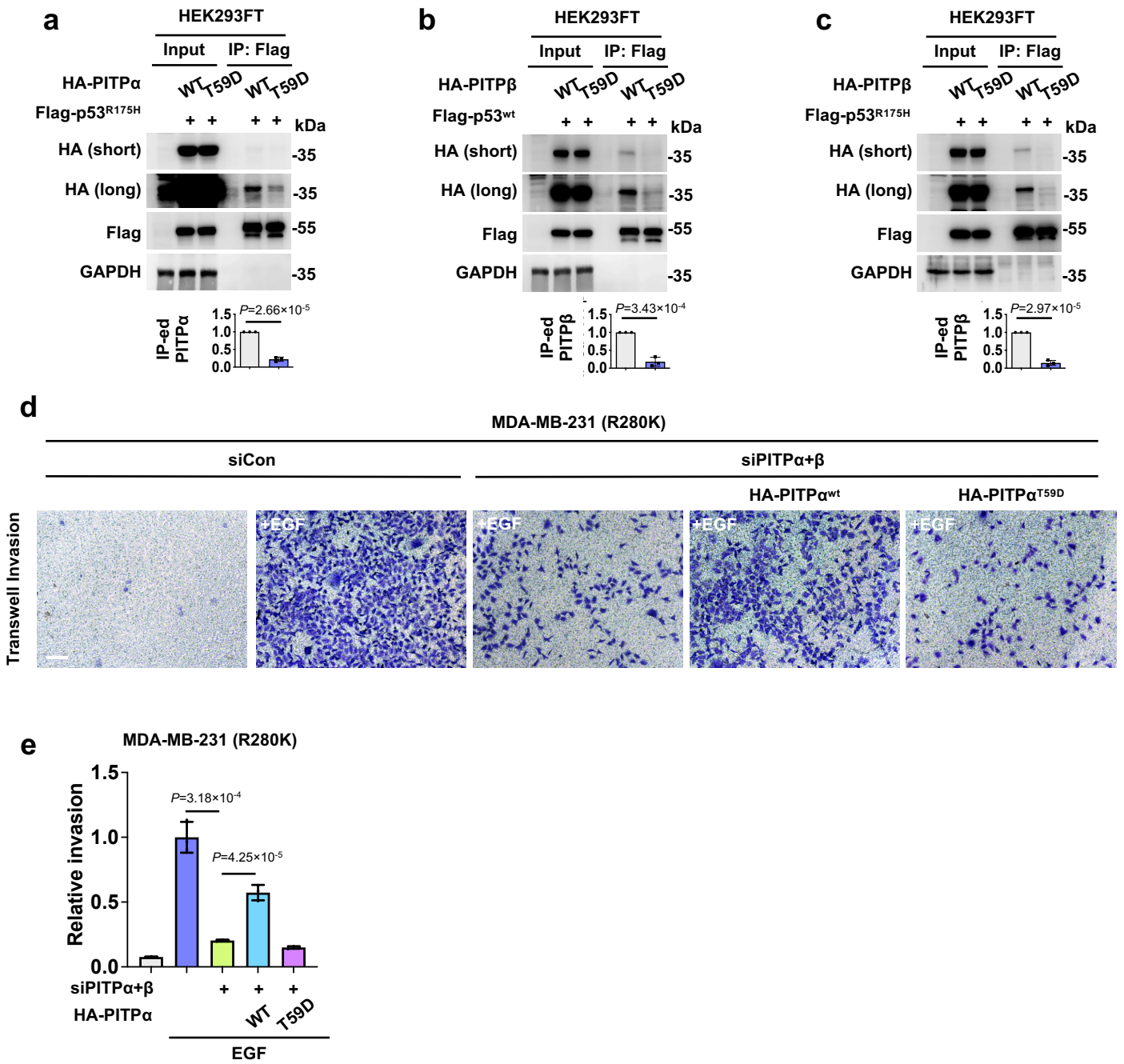

Extended Data Figure 9. PITPs require PI binding to function with p53

a, HEK293FT cells were co-transfected with either HA-tagged wild-type PITPα or PI binding-defective mutant T59D PITPα together with Flag-tagged mutant $p53^{R175H}$. After 48 h, cells were processed for IP against Flag-tag and analyzed by WB. *p* value denotes two-sided paired t-test. n=3 independent experiments.

b, HEK293FT cells were co-transfected with either HA-tagged wild-type PITPβ or PI binding-defective mutant T59D PITPβ together with Flag-tagged $p53^{wt}$. After 48 h, cells were processed for IP against Flag-tag and analyzed by WB. *p* value denotes two-sided paired t-test. n=3 independent experiments.

c, HEK293FT cells were co-transfected with either HA-tagged wild-type PITPβ or PI binding-defective mutant T59D PITPβ together with Flag-tagged mutant $p53^{R175H}$. After 48 h, cells were processed for IP against Flag-tag and analyzed by WB. *p* value denotes two-sided paired t-test. n=3 independent experiments.

d-e, MDA-MB-231 cells were transfected with control siRNAs or siRNAs against the 3'UTR of both PITPα and PITPβ for 24 h. The cells were then transfected with either HA-tagged wild-type PITPα or PI binding-defective mutant T59D PITPα. After 24 h, cells were serum starved for an additional 24 h and then scored for invasion through Laminin-coated transwell inserts with 8 μm pores using 10 ng/ml EGF as a chemoattractant for 16 h. The invading cells at the insert bottom were stained with Crystal Violet, imaged (**d**), and quantified (**e**) based on the extracted dye using a plate reader. n=3 independent experiments. *p* value denotes two-sided paired t-test. Scale bar, 300 μm.

For all graphs, data are presented as the mean ± SD.